AEDC-TR-76-34

cy 2

COMPARISON OF ELECTRON-ION RECOMBINATION AND GAS-DYNAMIC EXPANSION RATES IN FREELY EXPANDING HELIUM AND ARGON PLASMAS

ENGINE TEST FACILITY
ARNOLD ENGINEERING DEVELOPMENT CENTER
AIR FORCE SYSTEMS COMMAND
ARNOLD AIR FORCE STATION, TENNESSEE 37389

March 1976

Interim Report for Period July 1, 1973 — June 30, 1975

Approved for public release; distribution unlimited.

Prepared for

DIRECTORATE OF TECHNOLOGY (DY)
ARNOLD ENGINEERING DEVELOPMENT CENTER
AIR FORCE SYSTEMS COMMAND
ARNOLD AIR FORCE STATION, TENNESSEE 37389

NOTICES

When U. S. Government drawings specifications, or other data are used for any purpose other than a definitely related Government procurement operation, the Government thereby incurs no responsibility nor any obligation whatsoever, and the fact that the Government may have formulated, furnished, or in any way supplied the said drawings, specifications, or other data, is not to be regarded by implication or otherwise, or in any manner licensing the holder or any other person or corporation, or conveying any rights or permission to manufacture, use, or sell any patented invention that may in any way be related thereto.

Qualified users may obtain copies of this report from the Defense Documentation Center.

References to named commercial products in this report are not to be considered in any sense as an endorsement of the product by the United States Air Force or the Government.

This report has been reviewed by the Information Office (OI) and is releasable to the National Technical Information Service (NTIS). At NTIS, it will be available to the general public, including foreign nations.

APPROVAL STATEMENT

This technical report has been reviewed and is approved for publication.

FOR THE COMMANDER

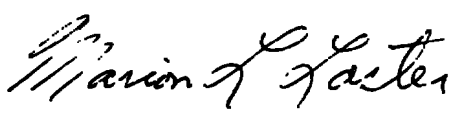

MARION L. LASTER
Research & Development
Division
Directorate of Technology

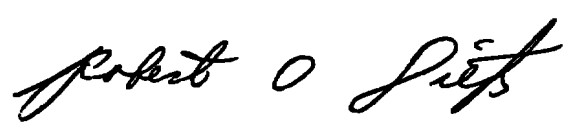

ROBERT O. DIETZ
Director of Technology

REPORT DOCUMENTATION PAGE		READ INSTRUCTIONS BEFORE COMPLETING FORM
1 REPORT NUMBER AEDC-TR-76-34	2 GOVT ACCESSION NO.	3 RECIPIENT'S CATALOG NUMBER
4 TITLE (and Subtitle) COMPARISON OF ELECTRON-ION RECOMBINATION AND GAS-DYNAMIC EXPANSION RATES IN FREELY EXPANDING HELIUM AND ARGON PLASMAS		5 TYPE OF REPORT & PERIOD COVERED Interim Report-July 1, 1973-June 30, 1975 6 PERFORMING ORG REPORT NUMBER
7 AUTHOR(s) L. H. Malone, University of Tennessee Space Institute, and C. C. Limbaugh, ARO, Inc.		8 CONTRACT OR GRANT NUMBER(s)
9 PERFORMING ORGANIZATION NAME AND ADDRESS Arnold Engineering Development Center (DY) Air Force Systems Command Arnold Air Force Station, Tennessee 37389		10 PROGRAM ELEMENT, PROJECT, TASK AREA & WORK UNIT NUMBERS Program Element 65807F
11 CONTROLLING OFFICE NAME AND ADDRESS Arnold Engineering Development Center (DYFS) Air Force Systems Command Arnold Air Force Station, Tennessee 37389		12. REPORT DATE March 1976 13. NUMBER OF PAGES 52
14 MONITORING AGENCY NAME & ADDRESS(if different from Controlling Office)		15. SECURITY CLASS. (of this report) UNCLASSIFIED 15a. DECLASSIFICATION/DOWNGRADING SCHEDULE N/A

16 DISTRIBUTION STATEMENT (of this Report)

Approved for public release; distribution unlimited.

17 DISTRIBUTION STATEMENT (of the abstract entered in Block 20, if different from Report)

18 SUPPLEMENTARY NOTES

Available in DDC

19. KEY WORDS (Continue on reverse side if necessary and identify by block number)

collisions	radiation
radiative transfer	arcjet engines
gas-dynamic phenomena	argon arc plasmas
plumes	helium

20. ABSTRACT (Continue on reverse side if necessary and identify by block number)

Equations coupling the collisional-radiative recombination and gas-dynamic phenomena for the centerline of the freely expanding plume of an argon and helium arcjet are developed and solved for the free electron density. The results of these calculations are used to ascertain the time rates of change of the free electron density attributable to the recombination and gas-dynamic processes separately. In this manner, and for the

DD FORM 1 JAN 73 1473 EDITION OF 1 NOV 65 IS OBSOLETE

20. ABSTRACT (Continued)

stagnation conditions examined, ($3,000^{\circ}K \leq$ total gas temperature $\leq 4,900^{\circ}K$, 1×10^{17} $cm^{-3} \leq$ electron number density $\leq 5 \times 10^{18}$ cm^{-3}, and $1,200^{\circ}K \leq$ electron temperature $\leq 20,000^{\circ}K$) it was determined that for all cases considered the gas-dynamic processes dominated the recombination processes beyond two nozzle exit diameters downstream in the plume. Experimental data are presented which support the conclusions drawn from the analytical results. Therefore, based on these results, a more detailed approach than the collisional-radiative recombination model is necessary for the correct description of recombination mechanisms in the rapidly changing environment of the expanding arcjet plume.

APSC
Arnold AFS Tenn

PREFACE

The research reported herein was conducted by the Arnold Engineering Development Center (AEDC) under Program Element 65807F. The results of this research program were obtained by ARO, Inc. (a subsidiary of Sverdrup & Parcel and Associates, Inc.), contract operator of AEDC, Air Force Systems Command (AFSC), Arnold Air Force Station, Tennessee. The work was accomplished in the Engine Test Facility (ETF) under ARO Project Numbers RF413 and R33A-00A. The manuscript (ARO Control No. ARO-ETF-TR-75-114) was submitted for publication on June 30, 1975.

The authors of this report, L. H. Malone, University of Tennessee Space Institute and C. C. Limbaugh, ARO, Inc., wish to express appreciation to Dr. W. K. McGregor, ARO, Inc., discussions with whom provided the basis for this study, and to R. J. Bryson and J. D. Few, ARO, Inc., for their technical advice and information.

CONTENTS

ILLUSTRATIONS

Figure

TABLES

1.0 INTRODUCTION

1.1 OBJECTIVE

In the past several years, the use of partially ionized gases, commonly called plasmas, in the research and test environment has become commonplace. These plasmas occur in such diverse applications as arc-heated wind tunnels, lasers, electron beam diagnostics, reentry, and radiofrequency (RF) heaters. The manner of treatment of the plasma state usually employed is to express the gross properties of flows in terms familiar for un-ionized gases, and at the same time account for the observables peculiar to the plasma state. The bulk gas properties may still be expressed as pressure, temperature, density, etc., while the plasma properties are defined in terms of electron density, recombination rate, etc.

Because the electron-ion recombination process is necessarily a collisional one, it is generally described through the use of a recombination rate coefficient. The recombination rate coefficient is related to the probability of the occurrence of a successful recombination event, integrated over the energy distribution function of the collision partners. Because some cross sections (probabilities) are very difficult and others are impossible to obtain directly from theory, the rate coefficients are generally obtained through experimental means. Although recombination rate coefficient determinations have been the subject of numerous investigations, the measurements are often compromised or made more difficult by the short plasma life time of by containment effects.

The present work is an examination of the processes affecting the electron number density along the centerline of the freely expanding plasma. The time rates of change of the electron density attributable to the gas dynamic and recombination mechanisms are compared to ascertain the utility of a simple approach of determining the recombination rate coefficient. This approach requires only the determination of the electron number density at points along a streamline of the freely expanding plasma, as, for example, the centerline of an arcjet plume. To be successful, the recombination rate must necessarily dominate the time rate of change of the electron number density attributable to gas-dynamic processes. The examination of the relative magnitude of these two rates constitutes the major portion of this report.

1.2 BACKGROUND

1.2.1 Experimental Determination of Recombination Rates

Determining the value of the electron-ion recombination rate coefficient, α, for different gases has been the subject of numerous studies (Refs. 1 through 11). In 1896, Thomson and Rutherford made the first studies of recombination (Ref. 1) and proposed the mechanism of recombination to explain the gradual decrease in the conductivity of a gas following its ionization by a burst of X-rays. Various experimental techniques have since been used to determine the recombination rate coefficient. Difficulties in experimentally determining α are due to the loss of electrons from a measurement volume by diffusion as well as recombination (Ref. 1).

Effective measurements of helium recombination rate coefficients by Biondi and Brown (Refs. 2 and 3) utilized microwaves to ionize the sample gas as well as a means for measurement. These measurements depended upon obtaining the mean decay time of charge density following breakdown in a container of known dimensions. Diffusion and wall recombination effects were present, and it was necessary to account for them. Oskam (Ref. 4) analyzes some of the shortcomings of this approach. Despite these disadvantages, other investigators, including Redfield and Holt (Ref. 5), Oskam and Mittelstadlt (Ref. 6), and Chen (Refs. 7, 8) have used the approach for ascertaining the recombination rate coefficients for the rare gases He, Ne, Ar, Kr, and Xe. Other investigators are cited in Ref. 1.

Another approach which has been used successfully in recent years for both helium and argon is that of laser interferometry. The laser work, pioneered by Gusinow, Gerardo, and Verdeyen (Ref. 9) uses a plasma produced in a laser cavity. The resultant change in the laser frequency caused by the presence of the electrons yields the necessary data for the recombination rate coefficient determination. Their procedure uses the refractivity of the plasma at optical wavelengths and the expression deduced by Gerardo and Verdeyen (Ref. 10). The experiment also requires accounting for diffusion effects.

Another approach in recent years has been to use spectroscopic techniques to obtain the fundamental data necessary to ascertain the recombination rate coefficients. This approach, illustrated for example by the work of Shirai and Tabei (Ref. 11), builds upon an analytic technique first suggested by Byron, Stabler, and Bortz (Ref. 12) and requires detailed measurement of absolute spectral intensities as well as a

detailed calculational procedure. Shirai and Tabei used as their plasma source the freely expanding plume from a helium arcjet, thus showing the basic feasibility of the experimental approach. Their approach requires measurement of the intensities of spectral lines originating from the several excited states and relating these to the absolute number densities of each energy level. The number densities can then be related to the collisional cross sections and thence to the recombination rate coefficient.

An alternative possibility, much simpler in concept, is to determine the free electron number density at successive points along the centerline of the plume from the arcjet. This number density, along with an accounting of the flow velocity, allows the average rate of change of the free electron number density to be calculated and thence, related to the recombination rate coefficient.

1.2.2 Theoretical Calculations

Several approaches have also been taken to determine theoretically the recombination rate coefficient for helium and argon. One of the methods is a solution of the quasi-equilibrium equations for collision-radiative recombination as proposed by Bates, Kingston, and McWhirter (Ref. 13). This method, descriptive of the physical processes involved, will be discussed in more detail in a subsequent section and was used by Drawin (Ref. 14) to obtain recombination rate coefficients for helium. Drawin's results are used in the present study for theoretical helium calculations coupling the gas-dynamic and recombination processes.

In a second method, proposed by Byron, Stabler, and Bortz (Ref. 12), the principle is used that under equilibrium conditions there exists a pronounced minimum in the total rate of de-excitation of atoms as a function of the principal quantum number of the excited state. This minimum limits the net rate of three-body recombination to the rate of de-excitation of the level at which the minimum occurs. Using this simpler calculational method in the hydrogenic approximation, Wanless (Ref. 15), obtained argon recombination rate coefficients in agreement with the experimental values of Chen (Ref. 7). Since Wanless' results agree with the more complex method and cover a wide range of electron temperatures and electron densities, they are used in the present study for theoretical argon calculations coupling the gas-dynamic and recombination processes.

2.0 THEORY

2.1 INTRODUCTION

The description of the free expansion of a partially ionized gas from an arcjet involves two distinct, yet coupled, physical phenomena. Recombination processes are continually providing for the adjustment of the number densities of the charged specie (free electrons and singly charged ions for the purposes of this study). The gas-dynamic processes involved in the rapid expansion of the gas from a reservoir causes the number densities to decrease with increasing distance from the reservoir. Since the description of each phenomenom involves quantities affected by the other, a theoretical description of the processes must include considerations for superposing the two phenomena. In this section, the equations describing recombination and gas-dynamic processes are discussed, as well as the technique used for superposing the two processes.

2.2 COLLISIONAL-RADIATIVE RECOMBINATION

The initial work on a broad description of electron-ion recombination was done by Bates, Kingston, and McWhirter (Ref. 13) for optically thin and optically thick hydrogenic plasmas. For the case of an optically thin plasma, they confined their discussion to the recombination of electrons (denoted by e^-) with bare nuclei (denoted by N^+) of charge Ze (where Z is the level of ionization and e is the charge on an electron) to form hydrogen atoms or hydrogenic ions. Letting p, q denote the quantum numbers of the discrete levels and letting c represent the continuum, the number densities of atoms or ions in the indicated levels are denoted by n(p), n(q). The number density of free electrons are designated by n(c) and the ions $n(N^+)$.

The collisional excitation or de-excitation process, which can be written

$$n(p) + e^- \rightarrow n(q) + e^-$$

is described with K(p, q) as the rate coefficient. Radiative recombination,

$$n(N^+) + e^- \rightarrow n(p) + h\nu$$

is described by the rate coefficient $\beta(p)$. Three-body recombination into some state p is described by the rate coefficients K(c, p), and the reverse ionizing process by the rate coefficient K(p, c). The three-body reaction is written

$$n(N^+) + e^- \rightleftarrows n(p) + e^-$$

The spontaneous radiative transition probability for the reaction

$$n(p) \rightarrow n(q) + h\nu$$

is denoted by A(p, q).

With the assumptions: (1) that the electronic transitions caused by atom-atom, atom-ion, or ion-ion collisions can be neglected; (2) boundary effects can be neglected; and (3) the plasma is optically thin so that all emitted radiation escapes the plasma without being absorbed, Bates et al. (Ref. 13) were able to express the rate of change of n(p) with time by

$$\begin{aligned}\frac{dn(p)}{dt} = & -n(p)\left[n(c)K(p,q) - n(c)\sum_{q\neq p}K(p,q) + \sum_{q<p}A(p,q)\right] \\ & + n(c)\sum_{q\neq p}n(q)K(q,p) + \sum_{q>p}n(q)A(q,p) \\ & + n^2(c)[K(c,p) + \beta(p)]\end{aligned} \tag{1}$$

The terms in Eq. (1) can be identified, respectively, as depopulation caused by collisional ionization, collisional excitation, or de-excitation from state p to some other q^{th} state, radiative decay from state p to state q, population of state p caused by collisional excitation or de-excitation from some other q^{th} state, radiative decay to state p from some higher state q, three-body recombination into state p, and radiative recombination into state p. Thus, Eq. (1) forms the algebraic combination of all the rates that add to or subtract from the number density of atoms in level p. It should be noted that, in the formulation of Eq. (1), if a particular effect or transition is not allowed, the corresponding rate coefficient would be zero. If one thus writes an equation of the type represented by Eq. (1) for each state available to the plasma, one has at hand the complete transient description for the plasma decay. The solution to that problem has been attacked elsewhere (Ref. 16).

However, following Bates, et al. (Ref. 1), assuming that a quasi-steady-state condition (all rates are negligible except dn(1)/dt and

dn(c)/dt) is established almost instantaneously, and utilizing certain equilibria considerations, the system of equations represented by Eq. (1) can be replaced by the equation

$$\frac{dn(1)}{dt} = \Gamma n(c)n(N^+) \tag{2}$$

for single ionization. Equation (2) expresses the time rate of change of the population of the ground state, n(1), of the atom and depends upon the time rate of change of all other quantum states being negligibly small compared to that of the ground state and the free electron density. In Eq. (2), Γ can be written as

$$\Gamma = \alpha - S\frac{n(1)}{n(c)} \tag{3}$$

where α is called the collisional-radiative recombination (CRR) rate coefficient, and S is the collisional-radiative ionization (CRI) rate coefficient. Continuing with the results of Bates, et al., and substituting Eq. (3) into Eq. (2), one obtains

$$\frac{dn(1)}{dt} = \alpha n(c)n(N^+) - S\,n(1)n(N^+) \tag{4}$$

which yields dn(1)/dt in terms of α and S. For the conditions encountered in this study, the terms resulting from CRI are negligibly small and are thus neglected through the remainder of this work. For example, at an electron temperature of 10,000°K, an atom density on the order of 10^{18} cm^{-3}, and assuming one-percent ionization, the CRR coefficient for helium is on the order of 10^{-11} cm^3/sec and the CRI coefficient for helium is on the order of 10^{-19} cm^3/sec (Ref. 14). This yields rates on the order of 10^{23} cm^{-3}/sec and 10^{15} cm^{-3}/sec for CRR and CRI, respectively.

Since the plasmas considered in this work are assumed to be singly ionized, the quasi-steady-state assumption yields the condition

$$\frac{dn(1)}{dt} = -\frac{dn(c)}{dt} \tag{5}$$

or

$$\frac{dn(c)}{dt} = -\alpha n^2(c) \tag{6}$$

In order to determine the recombination rate coefficient in the absence of other effects and using Eq. (6), the electron number density along with the time rate of change of number density is all that is necessary.

2.3 GAS DYNAMICS AND RECOMBINATION

In the free expansion of a singly ionized plasma from an arcjet, the change in the electron number density from one point to another along the plume centerline is due not only to recombination, but also to the gas-dynamic effects. The velocity of the flow can be used in relating time and position, so that in principle, a typical gas-dynamic (spatially dependent) description can be used in determining the time rate of change of the electron number density attributable to the expansion effects.

It has been shown that if the degree of ionization is small, conventional isentropic gas-dynamic theory should give a good approximation for macroscopic plasma properties (Ref. 17) in the arcjet plume, such as pressure, temperature, and density. Therefore (Ref. 18),

$$\frac{\rho}{\rho_o} = \left(1 + \frac{\gamma - 1}{2} M^2\right)^{-\frac{1}{\gamma-1}} \tag{7}$$

where γ is the ratio of specific heats ($\gamma = 1.67$ for noble gases), M is the Mach number ($M = V/c$, where V is the velocity of the flow and c is the speed of sound), ρ is the mass density at some point downstream of the nozzle, and ρ_o is the mass density at stagnation conditions. The mass density is directly proportional to the number of particles per unit volume; therefore, for two points in the flow

$$\left[\frac{n + n(N^+)}{n_o}\right]_1 = \left(1 + \frac{\gamma - 1}{2} M_1^2\right)^{\frac{1}{\gamma-1}}$$

$$\left[\frac{n + n(N^+)}{n_o}\right]_2 = \left(1 + \frac{\gamma - 1}{2} M_2^2\right)^{-\frac{1}{\gamma-1}} \tag{8}$$

where the numerator in the terms on the left expresses the number density of heavy particles at each of the two adjacent positions. It is assumed that the forces acting on the ions are principally gas dynamic in nature. Thus one can write

$$\frac{[n + n(N^+)]_2}{[n + n(N^+)]_1} = \left[\frac{1 + \frac{\gamma - 1}{2} M_1^2}{1 + \frac{\gamma - 1}{2} M_2^2}\right]^{\frac{1}{\gamma - 1}} \tag{9}$$

If it is assumed that the level of ionization is low,

$$n >> n(N^+)$$

the recombination process will not appreciably affect the atom number density. Thus, expanding Eq. (9) algebraically,

$$n_2 + n(N^+)_2 = f(M) n_1 + f(M) n(N^+)_1$$

where

$$f(M) = \left[\frac{1 + \frac{\gamma - 1}{2} M_1^2}{1 + \frac{\gamma - 1}{2} M_2^2}\right]^{\frac{1}{\gamma - 1}}$$

The terms involving the atom densities (the first terms on each side of the equation) can be cancelled and one can write, approximately for only the gas-dynamic effects on the ion density,

$$\frac{n(N^+)_2}{n(N^+)_1} = \left[\frac{1 + \frac{\gamma - 1}{2} M_1^2}{1 + \frac{\gamma - 1}{2} M_2^2}\right]^{\frac{1}{\gamma - 1}} \tag{10}$$

It is further assumed that the ions are singly ionized. It can then be shown that, at the conditions of this work, the Debye length is much shorter than the nozzle exit diameter so that there is no charge separation and the plasma is electrically neutral locally. Thus the gas-dynamic

effects upon the ions also describes the gas-dynamic effects upon the free electrons. The ion and electron number densities are further depleted by the effects of recombination. This can be accounted for by including the integrated effects of the recombination, or

$$\frac{n(c)_2}{n(c)_1} = \left[\frac{1 + \frac{\gamma - 1}{2} M_1^2}{1 + \frac{\gamma - 1}{2} M_2^2}\right]^{\frac{1}{\gamma - 1}} - \frac{1}{n(c)_1} \int_{t_1}^{t_2} \alpha n^2(c) dt \tag{11}$$

If the two points are sufficiently close together, the integral may be closely approximated by the finite difference form and one can write

$$n(c)_2 = n(c)_1 \left[\frac{1 + \frac{\gamma - 1}{2} M_1^2}{1 + \frac{\gamma - 1}{2} M_2^2}\right]^{\frac{1}{\gamma - 1}} - 1/2 \left[n(c)_2^2 \alpha_2 + n(c)_1^2 \alpha_1\right](t_2 - t_1) \tag{12}$$

where the second term is the contribution of the recombination process. As was described in Section 2.2, α is an implicit function of electron number density and electron temperature, and Eq. (12) can be solved iteratively for $n(c)_2$ provided conditions at position one and the M_2 are known.

With $n(c)_2$ determined and assuming that conditions at position one are constant as view from position two, the time derivative of $n(c)_2$ is

$$\frac{dn(c)_2}{dt} = - n(c)_1 \left(1 + \frac{\gamma - 1}{2} M_1^2\right)^{\frac{1}{\gamma - 1}} \left(1 + \frac{\gamma - 1}{2} M_2^2\right)^{-\frac{\gamma}{\gamma - 1}} M_2 \frac{dM_2}{dt} - \alpha\, n(c)_2^2 \tag{13}$$

Thus the rate of change of n(c) attributable to the gas-dynamic effect is

$$\left(\frac{dn(c)}{dt}\right)_G = - n(c)_1 \frac{\left(1 + \frac{\gamma - 1}{2} M_1^2\right)^{\frac{1}{\gamma - 1}}}{\left(1 + \frac{\gamma - 1}{2} M_2^2\right)^{\frac{\gamma}{\gamma - 1}}} M_2 \frac{dM_2}{dX_2} \frac{dX_2}{dt} \tag{14}$$

and, as before, the rate of change attributable to recombination is

$$\left(\frac{dn(c)}{dt}\right)_{CRR} = -\alpha\, n(c)_2^2$$

The M_2 in Eqs. (12) and (14) is required for the solution of $n(c)_2$ and a comparison of the rates attributable to the gas-dynamic expansion process. A. B. White (Ref. 19) has determined that the centerline Mach number distribution for the arcjet is adequately determined by the model proposed by Ashkenas and Sherman (Ref. 20). This model is used for determining M_2 and dM_2/dX in this study and is expressed by

$$M_2 = A\left(\frac{X_2}{D} - \frac{X_o}{D}\right)^{\gamma-1} - \frac{1/2\left(\frac{\gamma+1}{\gamma-1}\right)}{A\left(\frac{X_2}{D} - \frac{X_o}{D}\right)^{\gamma-1}} + \frac{C}{\left(\frac{X_2}{D} - \frac{X_o}{D}\right)^{3(\gamma-1)}} \qquad (15)$$

where A, C, and X_o/D are empirical constants determined by Ashkenas and Sherman by comparisons to the method of characteristics solutions. The distance from the exit plane of the nozzle is denoted by X_2 and the exit diameter by D. For a γ of 1.67, Ashkenas and Sherman determined A to be 3.26, C to be 0.31, and X_o/D to be 0.0075.

Differentiation of Eq. (15) with respect to X_2 yields dM_2/dX_2. The velocity of the flow at X_2 can be written as

$$V_2 = \frac{dX_2}{dt} = M_2 c \qquad (16)$$

where c is the speed of sound, and for an isentropic process using the equation of state,

$$\frac{dX_2}{dt} = M_2(\gamma R T_{g_2})^{1/2} \qquad (17)$$

where R is the gas constant, T_{g_2} is the static gas temperature at position 2, and

$$T_{g_2} = \frac{T_o}{1 + \frac{\gamma-1}{2} M_2^2} \qquad (18)$$

where T_o is the stagnation temperature.

2.4 METHOD OF SOLUTION

The analytic description of the coupled gas-dynamic and recombination processes developed in the preceding sections was solved to provide an estimate of the comparison of the electron number density decay rates by the two processes. The solution proceeds as a series of initial value problems, each solution providing the initial value for the next solution. Since the Ashkenas-Sherman model is valid only for $X/D \geq 1.0$, this value, 1.0, was chosen for the starting point and a time of 1×10^{-9} sec was arbitrarily associated with this point.

To effect the solution, an X_2 is chosen and from this, M_2, T_{g_2}, and dX_2/dt, are calculated [Eqs. (15), (18), and (17)]. These values are used to determine the average elapsed time from position one to position two:

$$\overline{\Delta t} = \frac{X_2 - X_1}{1/2\left[\frac{dX_2}{dt} + \frac{dX_1}{dt}\right]} \tag{19}$$

If this average elapsed time is greater than a predetermined fraction of the total time elapsed from the start of the calculations, 0.1 in this work, X_2 is reduced and a new average is computed. When the average time becomes less than the aforementioned fraction, $n(c)_2$ is determined, Eq. (12).

In this manner, for economy of computation, the time increment is kept small at the beginning of the calculations when conditions are changing rapidly but is allowed to increase as conditions change less rapidly. The rates of decay of electron density attributable to the gas-dynamic effects and the recombination are then calculated [Eqs. (14) and (16)] for comparison.

2.5 RECOMBINATION RATE COEFFICIENTS

The final parameter necessary to complete the calculations is the recombination rate coefficient. These data were taken from Wanless (Ref. 15) for argon and Drawin (Ref. 14) for helium. Wanless' results for argon were extrapolated graphically on a log-log plot of the recombination rate coefficient versus electron temperature at constant electron number density to provide the rate coefficients at electron number densities greater than 10^{16} cm^{-3} and electron temperatures greater than 16,000°K. The results of these graphical extrapolations are given in

Table 1. It was not necessary to extend the helium recombination coefficients from Drawin (Ref. 14). For use in the computer calculation, the graphical data were converted to tables and a three-point, two-dimensional Lagrangian interpolation was performed in the log-log plane to determine the recombination coefficient at a specific value of electron temperature and density.

Table 1. Extrapolated Values for Argon Recombination Coefficients

T_e, °K	n(c), $1/cm^3$	α, cm^3/sec
2,000	1×10^{17}	1.6×10^{-5}
2,000	1×10^{18}	1.6×10^{-5}
4,000	1×10^{17}	5.4×10^{-7}
4,000	1×10^{18}	7.6×10^{-6}
8,000	1×10^{17}	5.9×10^{-10}
8,000	1×10^{18}	9.4×10^{-10}
10,000	1×10^{17}	8.9×10^{-11}
10,000	1×10^{18}	1.2×10^{-10}
14,000	1×10^{17}	1.4×10^{-11}
14,000	1×10^{18}	1.6×10^{-11}
16,000	1×10^{17}	7.8×10^{-12}
16,000	1×10^{18}	8.2×10^{-12}
20,000	1×10^{10}	4.2×10^{-13}
20,000	1×10^{11}	4.5×10^{-13}
20,000	1×10^{12}	5.4×10^{-13}
20,000	1×10^{13}	7.4×10^{-13}
20,000	1×10^{14}	1.4×10^{-12}
20,000	1×10^{15}	1.4×10^{-12}
20,000	1×10^{16}	2.2×10^{-12}
20,000	1×10^{17}	3.8×10^{-12}
20,000	1×10^{18}	3.5×10^{-12}

3.0 RESULTS

3.1 CALCULATED RESULTS

The equations describing the coupled gas-dynamic and recombination mechanisms developed in the preceding section were solved for the electron number density along the centerline of a freely expanding, partially ionized helium and argon plume. The parameters necessary for the calculations are the electron temperature profile, the initial stagnation gas and electron density conditions, and the starting position in the plume. The electron temperature profiles used are described in the sections presenting results of the helium and argon calculations, and the other initial conditions, common to both gases, are presented in the next section.

3.1.1 Initial Conditions

The initial conditions required to obtain the solution to the coupled equations are the total gas temperature, the electron number density, and the starting position in the plume, X/D_o. As indicated earlier, the Ashkenas-Sherman model for Mach number is valid only for $X/D \geq 1.0$, so this value, 1.0, was chosen for X/D_o. Since the total gas temperature enters the calculations functionally as a square root and then only in the calculation of the gas velocity, the results of the calculations will be relatively insensitive to the value chosen. Thus the same total gas temperature, 3,000°K, was chosen for each of the calculations. This value is in the range of previous observations (Refs. 21 through 23) for argon. The calculations were done for a range of electron number densities and are listed in Table 2. Included in Table 2 are the initial values of electron number density at stagnation conditions, M = 0, and at the position, X/D = 1.

Table 2. Initial Values of Electron Number Density

M = 0	X/D = 1
1×10^{17} cm^{-3}	1.45×10^{16} cm^{-3}
5×10^{17} cm^{-3}	7.24×10^{16} cm^{-3}
1×10^{18} cm^{-3}	1.45×10^{17} cm^{-3}
5×10^{18} cm^{-3}	7.24×10^{17} cm^{-3}

3.1.2 Helium

The initial values for the electron number density listed in Table 2 were used to determine the solution to the coupled recombination and gas-dynamic equations for helium for two analytic models of the electron temperature decay. The first model,

$$T_e = 2540\ t^{-0.1} \tag{20}$$

is also used later for comparative calculations for argon and was chosen to simulate approximately the electron temperature characteristics observed in arcjet expansions. The second model,

$$T_e = 11\ t^{-0.392} \tag{21}$$

is similar in analytic form but describes a much faster electron temperature decay. Equation (21) was prompted by observing that the recombination rate coefficient is a decreasing function of electron temperature. Thus, on a comparative basis, the recombination effects would be much larger with an electron temperature characteristic modeled by Eq. (21) than when modeled by Eq. (20).

Typical results obtained for the helium expansions are shown in Figs. 1, 2, and 3 for the electron temperature model of Eq. (20). The left ordinate of each of these figures is the time rate of change of the free electron density attributable to the gas-dynamic and recombination effects. The abcissa is elapsed time. The scale along the top of the figures shows the corresponding X/D at the times listed on the abcissa. Included on each figure, utilizing the right ordinate, is a plot of α for the conditions of that calculation.

Figure 1 shows the results for an initial electron number density of 1×10^{17} cm^{-3}, Fig. 2 the results for an initial electron number density of 5×10^{17} cm^{-3}, and Fig. 3 the results for an initial electron number density of 1×10^{18} cm^{-3}. As can be seen, from these figures, recombination mechanisms dominate the decay only for the highest electron number density presented and then only early in the flow development. From the theory in Section 2.0 it was seen that the recombination rate is quadratically dependent upon the electron number density Eq. (6), whereas the gas-dynamic rate is linearly dependent upon the number density, Eq. (14). Hence, as indicated in these figures, one would expect the rapid rise in importance of recombination process with increasing electron number density. When recombination becomes dominant,

this quadratic dependence causes the free-electron number density to decay very rapidly until the gas-dynamic process once again dominates the time rate of change of the electron number density.

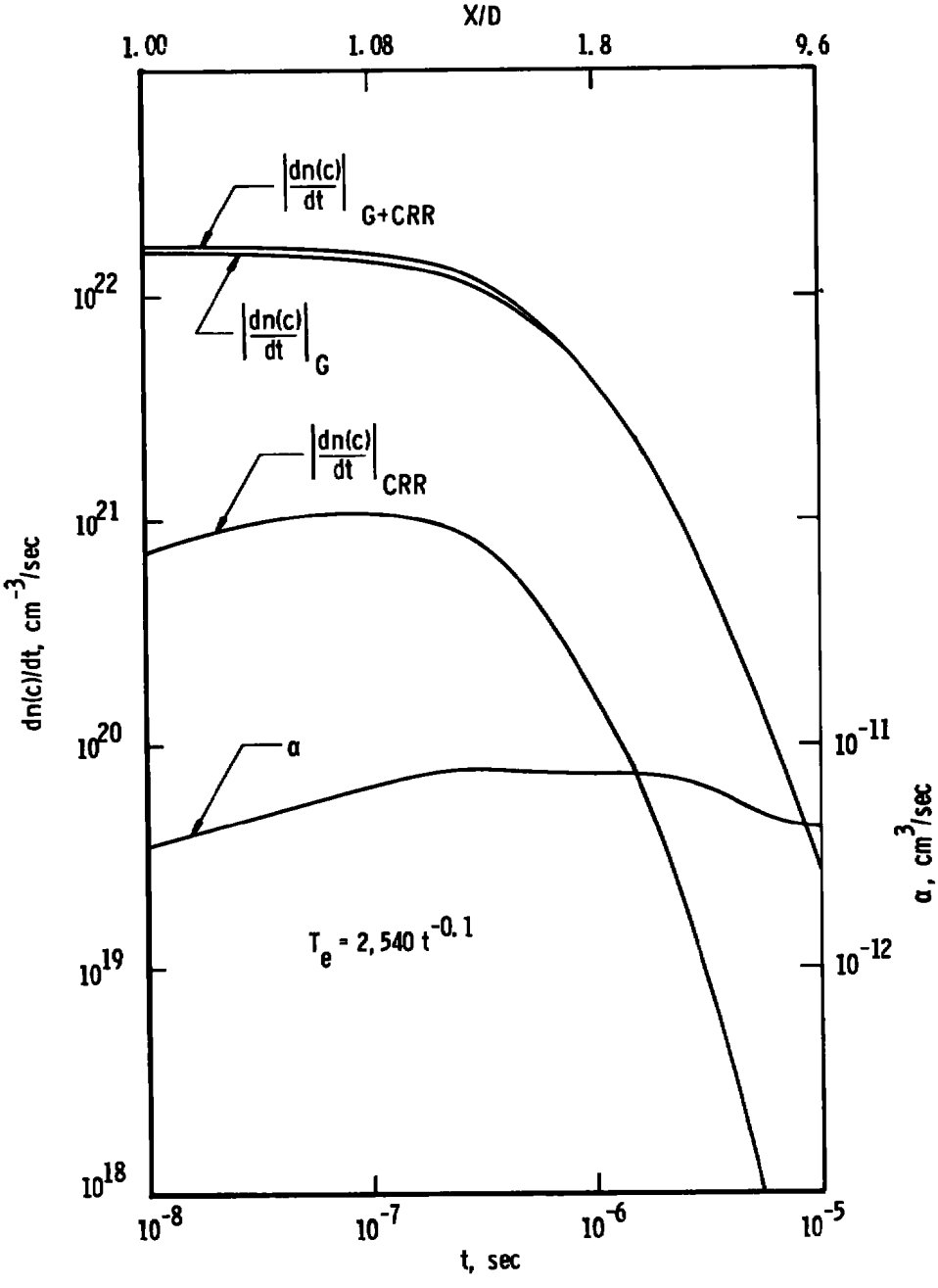

Figure 1. Time development of electron number density decay rates for helium expansion, $n(c)_o = 1 \times 10^{17}$ cm^{-3}.

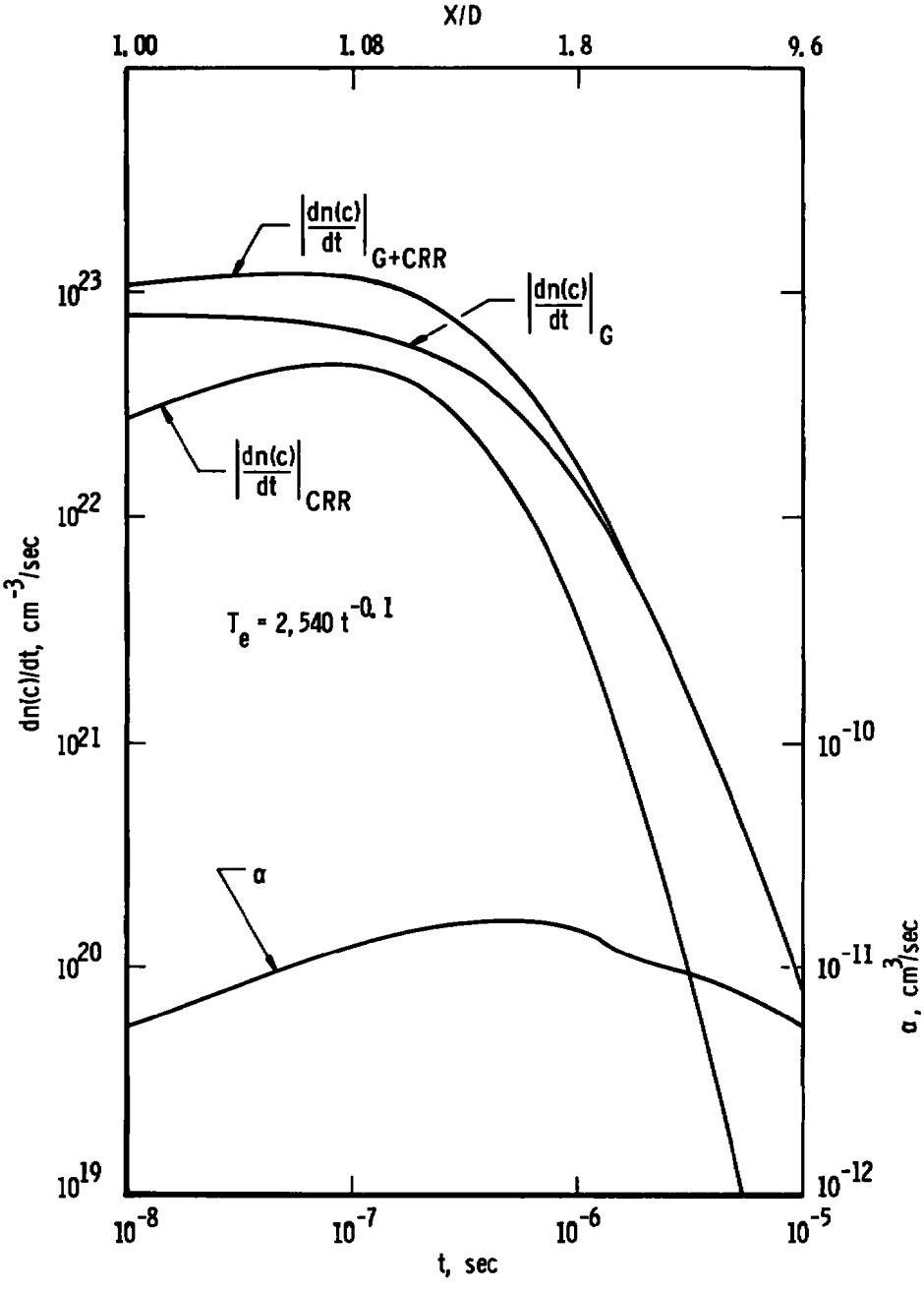

Figure 2. Time development of electron number density decay rates for helium expansion, $n(c)_o = 5 \times 10^{17}$ cm^{-3}.

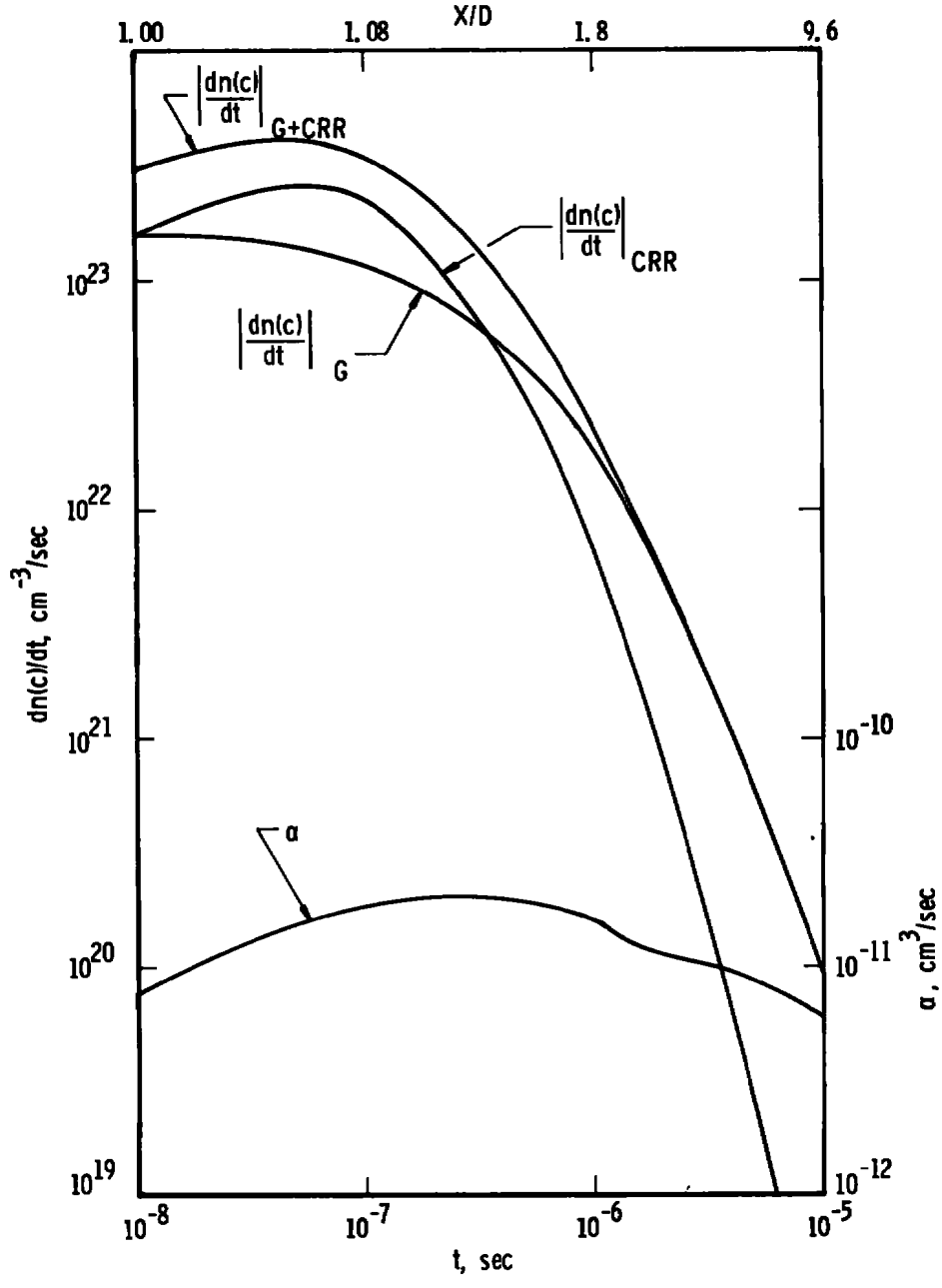

Figure 3. Time development of electron number density decay rates for helium expansion, $n(c)_o = 1 \times 10^{18}$ cm^{-3}.

The increasing rate of decay attributable to recombination during the early stages of the expansion ($t < 10^{-7}$ sec) is due to the increasing recombination rate coefficient with decreasing electron temperature. During this early time the integrated effect of the rates upon the electron density is insignificant and it remains essentially constant.

A more succinct and informative way of comparing the rate of electron density decay attributable to the recombination and gas-dynamic effects is by plotting the ratio of the recombination rate to the gas-dynamic rate versus X/D. In this manner, an ordinate greater than 1.0 signifies a dominance of the recombination mechanisms. These results for the electron temperature model of Eq. (20) are shown in Fig. 4. Thus, for the conditions of these calculations, the recombination mechanism is dominant in the decay only for the highest initial electron number densities ($(n(c)_o \geq 5 \times 10^{17}$ cm^{-3}) very close to the nozzle exit ($X/D \leq 1.4$). A plot of Eq. (20) is also included on Fig. 4 with the temperature scale given as the right ordinate.

If one-percent ionization is assumed, these conditions suggest that the total atom number density for such a helium expansion would be $n_o \geq 5 \times 10^{19}$, or, at 3,000°K, the total pressure would be greater than 150 torr. This is near the upper range operating conditions for the arcjet used for laboratory studies in this work. Figure 5 presents the results obtained at the same initial conditions but with the electron temperature model of Eq. (21). Because the electron temperature for these calculations falls much more rapidly with time [Eq. (21) as compared to Eq. (20)] one expects the recombination processes to have a much more dominant role. This is indeed the case as is shown in Fig. 5. The recombination dominates the entire decay for each of the initial electron number densities in the very early stages of the decay. However, the recombination rate invariably becomes dominated by the gas-dynamic rate a short distance downstream of the nozzle exit ($X/D < 2$).

An interesting feature of these calculations is that the ratio of the recombination rate to gas-dynamic rate approaches the same value as a function of X/D for a wide range of initial number densities. This is explained by the increase in recombination rate with electron number density at the same electron temperature when recombination dominates the gas-dynamic processes. Thus the electron number densities tend to the same X/D distribution. If this common distribution is reached before the gas-dynamic processes dominate the flow, the subsequent expansion proceeds at the same X/D distribution of densities, and the ratio of the recombination rate to gas-dynamic rate is the same for all initial electron number densities.

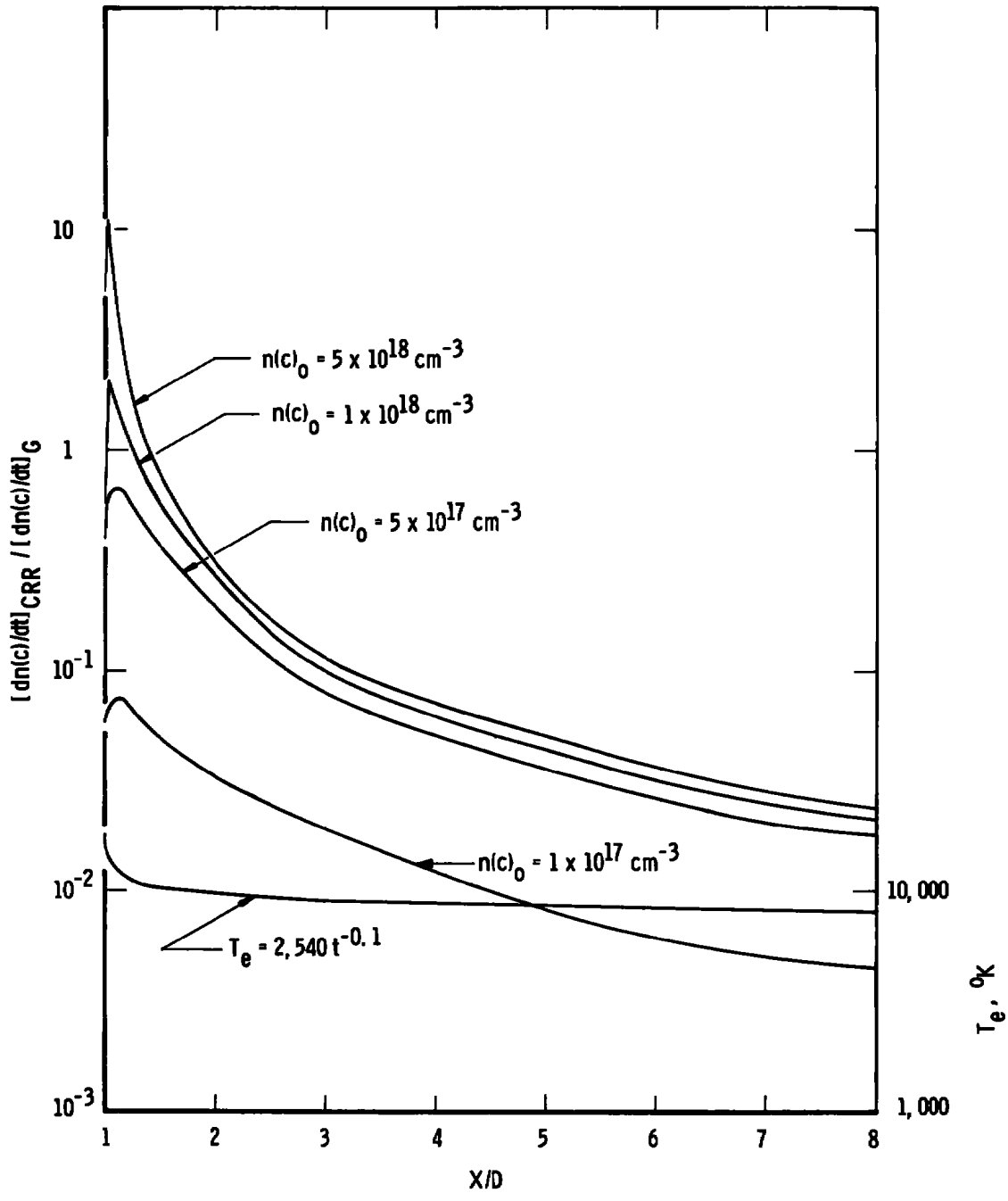

Figure 4. Comparison of electron number density decay rates attributable to recombination and gas dynamics, helium expansion, T_e modeled by slowly decaying function.

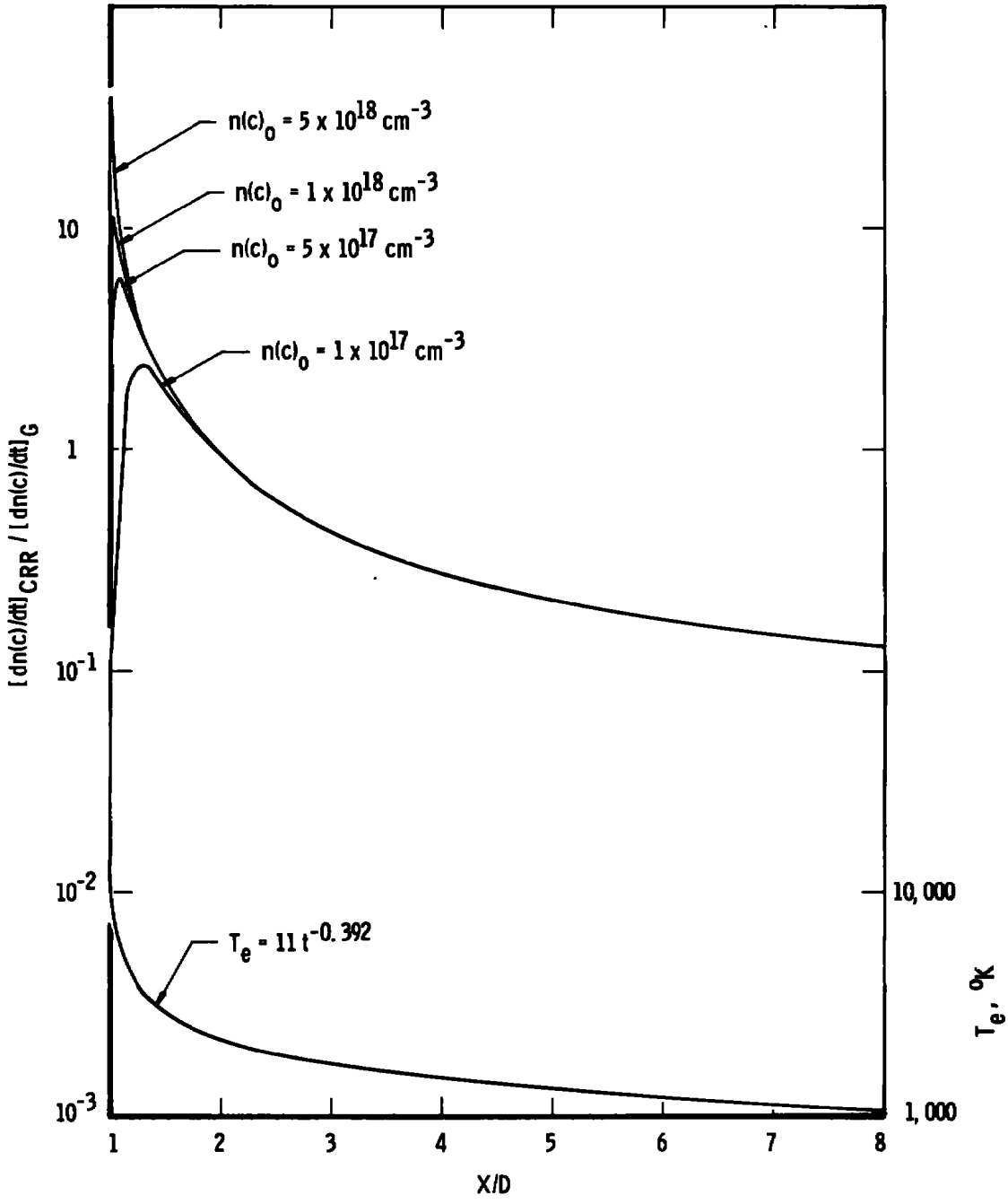

Figure 5. Comparison of electron number density decay rates attributable to recombination and gas dynamics, helium expansion, T_e modeled by rapidly decaying function.

If the gas-dynamic processes commence to dominate before the common X/D distribution is reached, the subsequent expansion proceeds at different electron number densities and thus a different ratio of recombination to gas-dynamic rate. That this is the case may be seen by comparing Figs. 4 and 5. In Fig. 4, the gas-dynamic rate dominated the expansion very early in the decay. For $X/D < 1.4$ it is seen that the plots for the two highest electron number densities were convergent. For $X/D > 1.4$, however, the spacing between the plotted lines tends to be constant. In Fig. 5 it is seen that the ratio of recombination rate to gas-dynamic rate converged to the same value at $X/D \approx 1.4$ for all but the lowest electron density. Calculations for $X/D > 1.4$ yield the same X/D distribution of electron number density.

3.1.3 Argon

The initial values for the electron number density listed in Table 2 were used to determine the solution of the coupled recombination and gas-dynamic equations for argon for two models of the electron temperature decay. The first of these is the same as was used for the helium calculations

$$T_e = 2540\, t^{-0.1} \tag{20}$$

and is useful for comparisons of the two gases. The second model was taken from McGregor and Brewer (Ref. 24) who presented experimental data from an argon arcjet. A graphical representation of the data from Ref. 24 is presented in Fig. 6.

The results of some of the calculations using Eq. (20) are shown in Figs. 7, 8, and 9, plotted in the same manner as Figs. 1, 2, and 3. A plot of α versus time is included in each figure.

Figure 7 shows the results obtained for an initial electron number density of 1×10^{17} cm^{-3}, Fig. 8 the results for an initial electron number density of 5×10^{17} cm^{-3}, and Fig. 9 shows the results for an initial number electron density of 1×10^{18} cm^{-3}. Comparison of these results with those of Figs. 1, 2, and 3 shows that the only essential difference is the X/D as a function of time. This is to be expected since the atomic weight of argon is 40 compared to 4 for helium and causes the helium velocity to be approximately three times that of argon; hence, the helium travels about three times as far as argon in the same time. The lower argon velocity causes the gas-dynamic

contribution to the time rate of change of the free-electron number density to be smaller than for helium. There are some differences in the rate attributable to recombination, also. Initially the differences are due to differences in the recombination rate coefficient for argon and helium and, as the flow develops, differences in the electron number density also contributes to the differences in the recombination rate. As with helium, once the gas-dynamic effects become the dominant mechanism, they remain so throughout the rest of the decay.

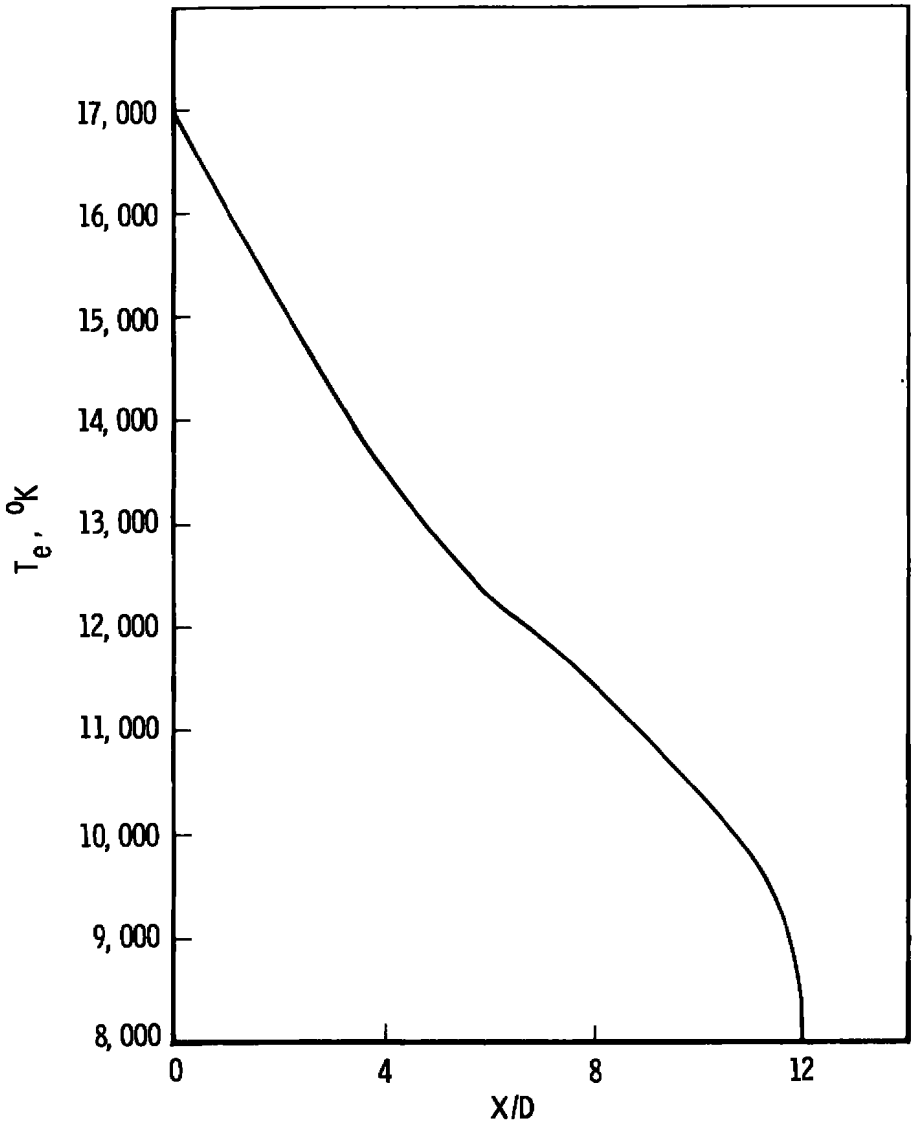

Figure 6. Centerline electron temperature profile, argon expansion (from Ref. 24).

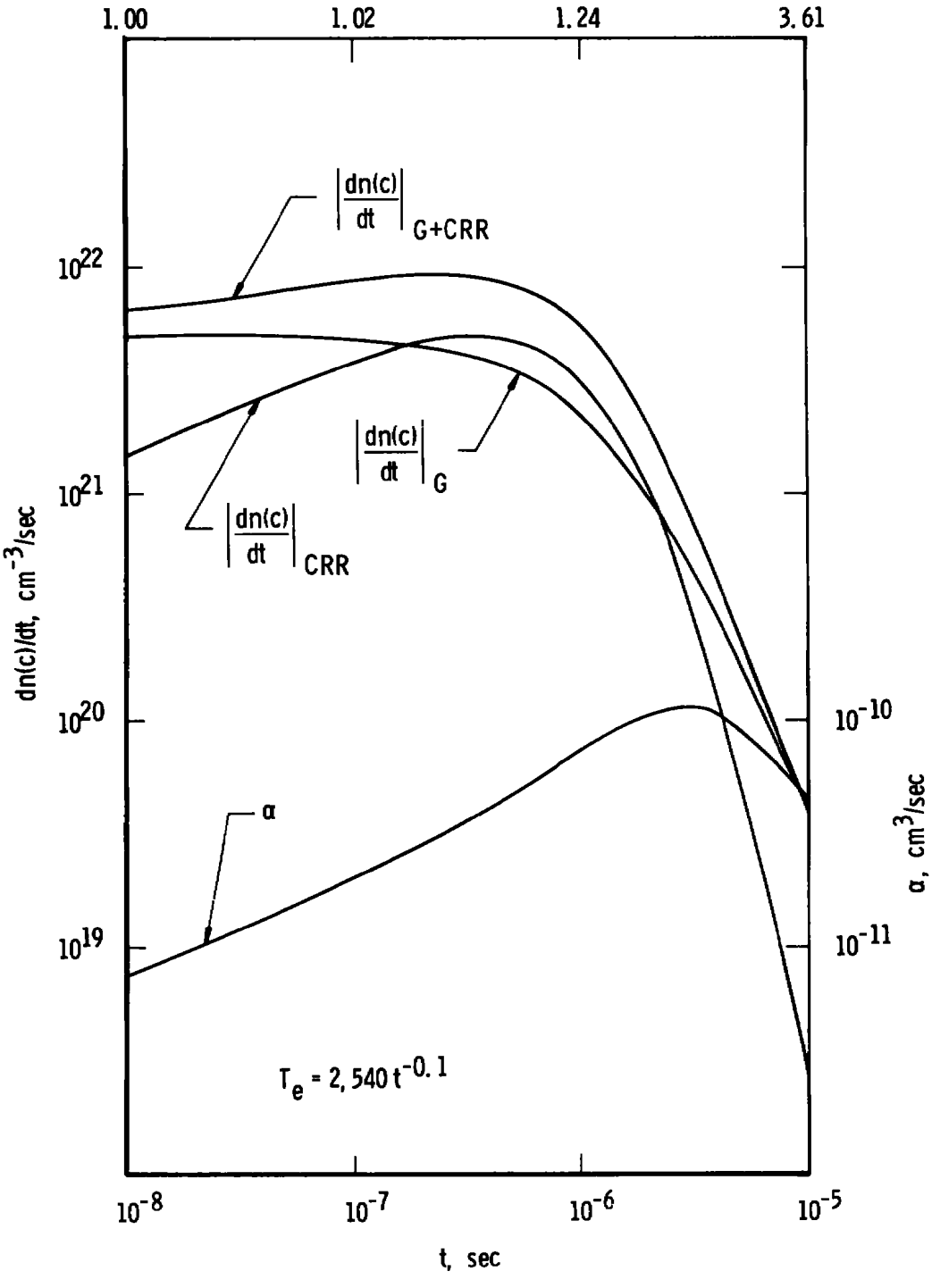

Figure 7. Time development of electron number density decay rates for argon expansion, $n(c)_o = 1 \times 10^{17}$ cm^{-3}.

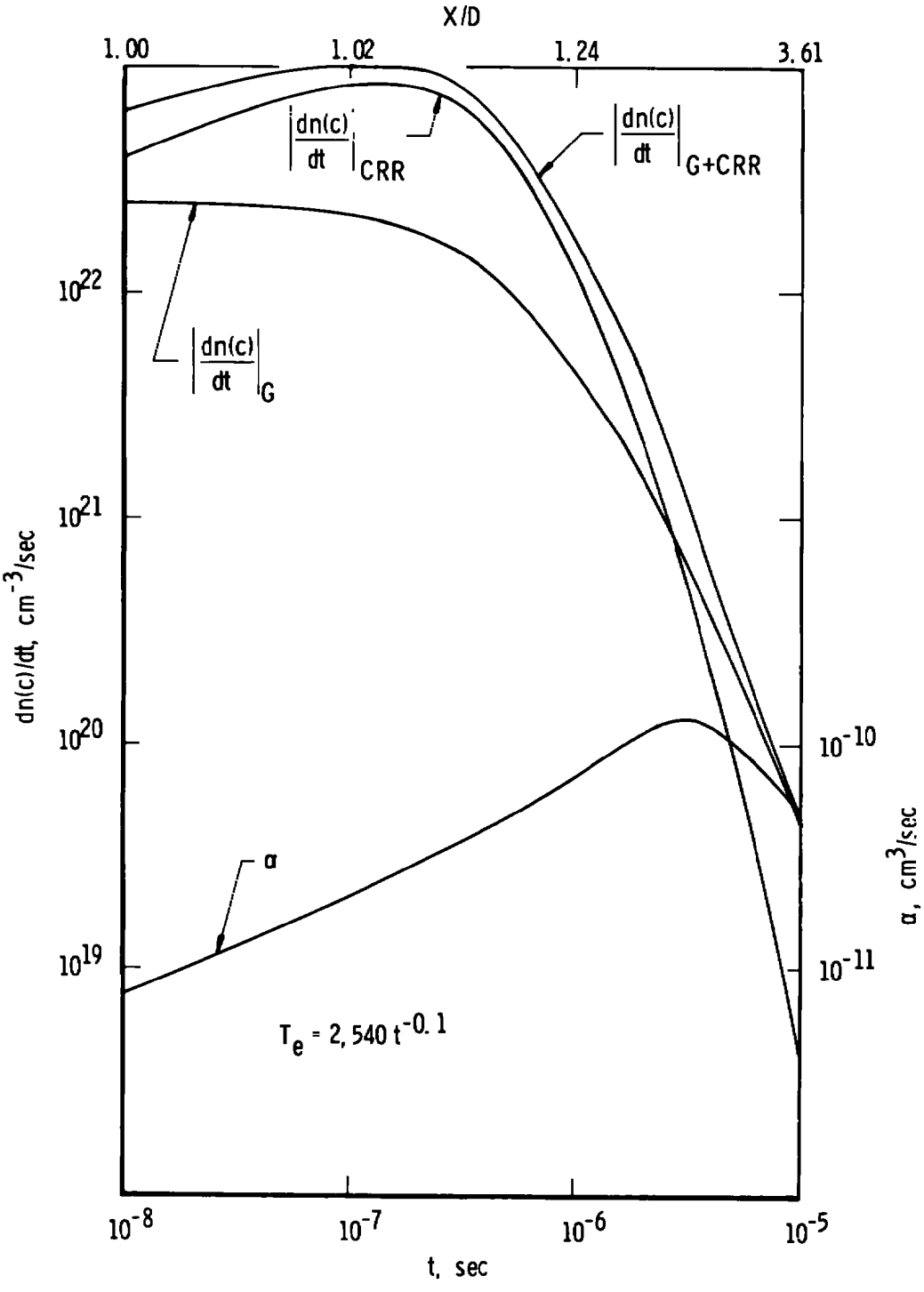

Figure 8. Time development of electron number density decay rates for argon expansion, $n(c)_o = 5 \times 10^{17}$ cm^{-3}.

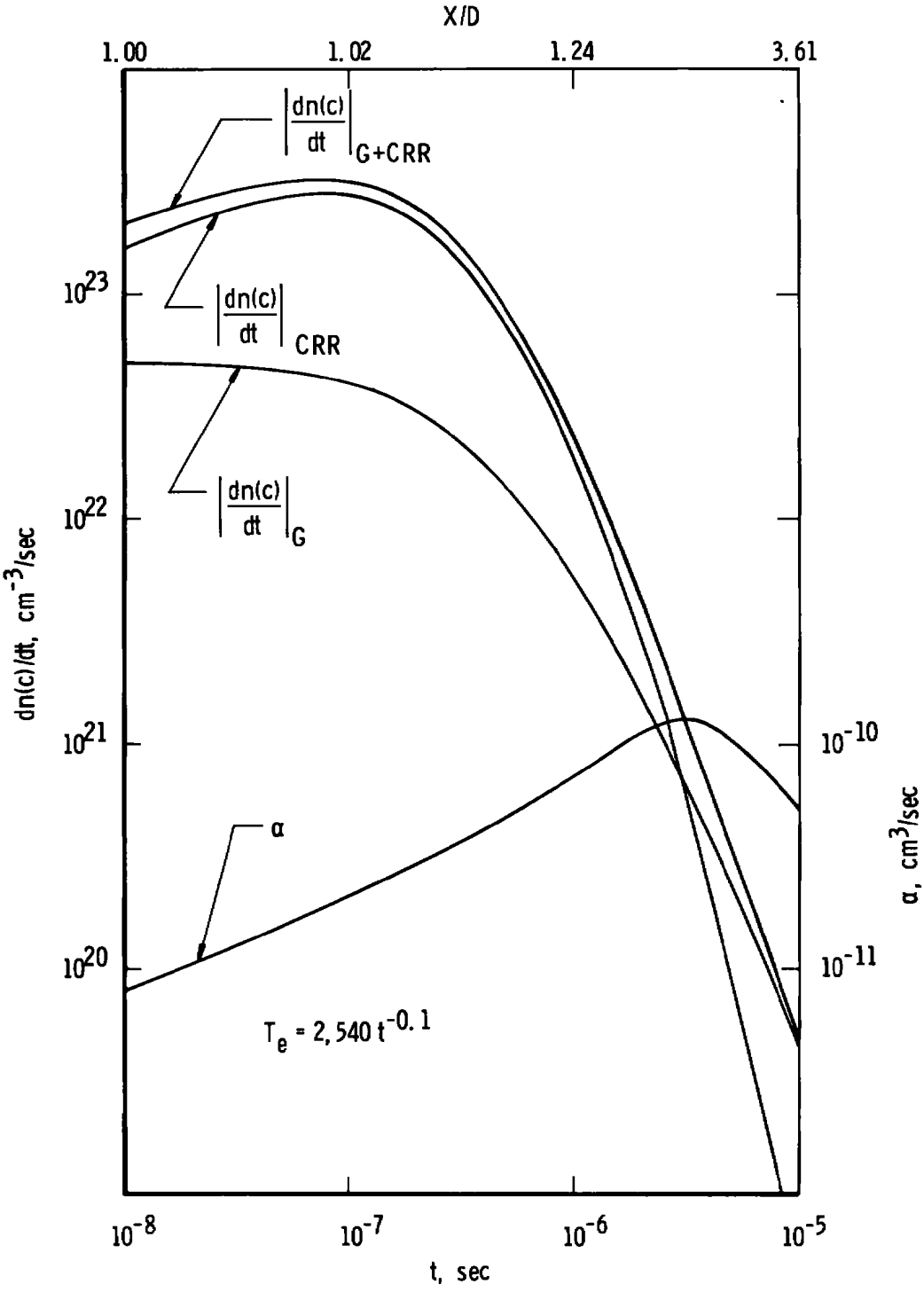

Figure 9. Time development of electron number density decay rates for argon expansion, $n(c)_o = 1 \times 10^{18}$ cm^{-3}.

The results of these calculations as well as the other initial conditions are summarized in Fig. 10. The ordinate is the ratio of the recombination rate of change of the electron number density to the gas-dynamic rate of change, and the abcissa is the axial distance from the nozzle exit, X/D. Comparisons of these results to those shown in Fig. 4 support the previous observations, with the adjustments appropriate to the different atomic weight. As with helium, the gas-dynamic processes dominate the expansion after the expansion reaches $X/D \approx 1.6$.

The results obtained from calculations based upon the electron temperature model reported in the literature (Ref. 24) and shown in Fig. 6, are shown in Fig. 11. For this profile also, as with the analytic model, Eq. (20), the gas-dynamic mechanisms dominate the decay for $X/D > 1.6$.

The calculations for helium and argon suggest strongly that, because of the contribution of the gas-dynamic processes, direct observation of the free-electron density is not sufficient for recombination rate coefficient determinations in the expanding arcjet plume. For the conditions used in this study, which are typical of those encountered in the laboratory, observation of the results shows that whenever the recombination mechanisms do dominate the decay, their nature is such that the electron density decays rapidly until the gas-dynamic processes become dominant.

3.2 EXPERIMENTAL DATA

The arcjet has been used in continuing research work at AEDC to investigate various excitation mechanisms. In the course of this work, heretofore unpublished data have been taken which can be used for comparisons with the results of the previous sections. In this section the procedures for obtaining the experimental data and the analysis will be discussed.

3.2.1 Apparatus and Procedure

The plasma jet used is of the Gerdien type and one model has been described in detail in Refs. 25 and 26. In the present study the plasma jet and other apparatus are most similar to that described in Ref. 26. Briefly, the arcjet consists of a hollow body into which the working gas is introduced. The plasma is produced in the arc region between a coaxial, water-cooled, tungsten cathode and a water-cooled, constant-area, copper nozzle anode. The plasma exhausts through this nozzle

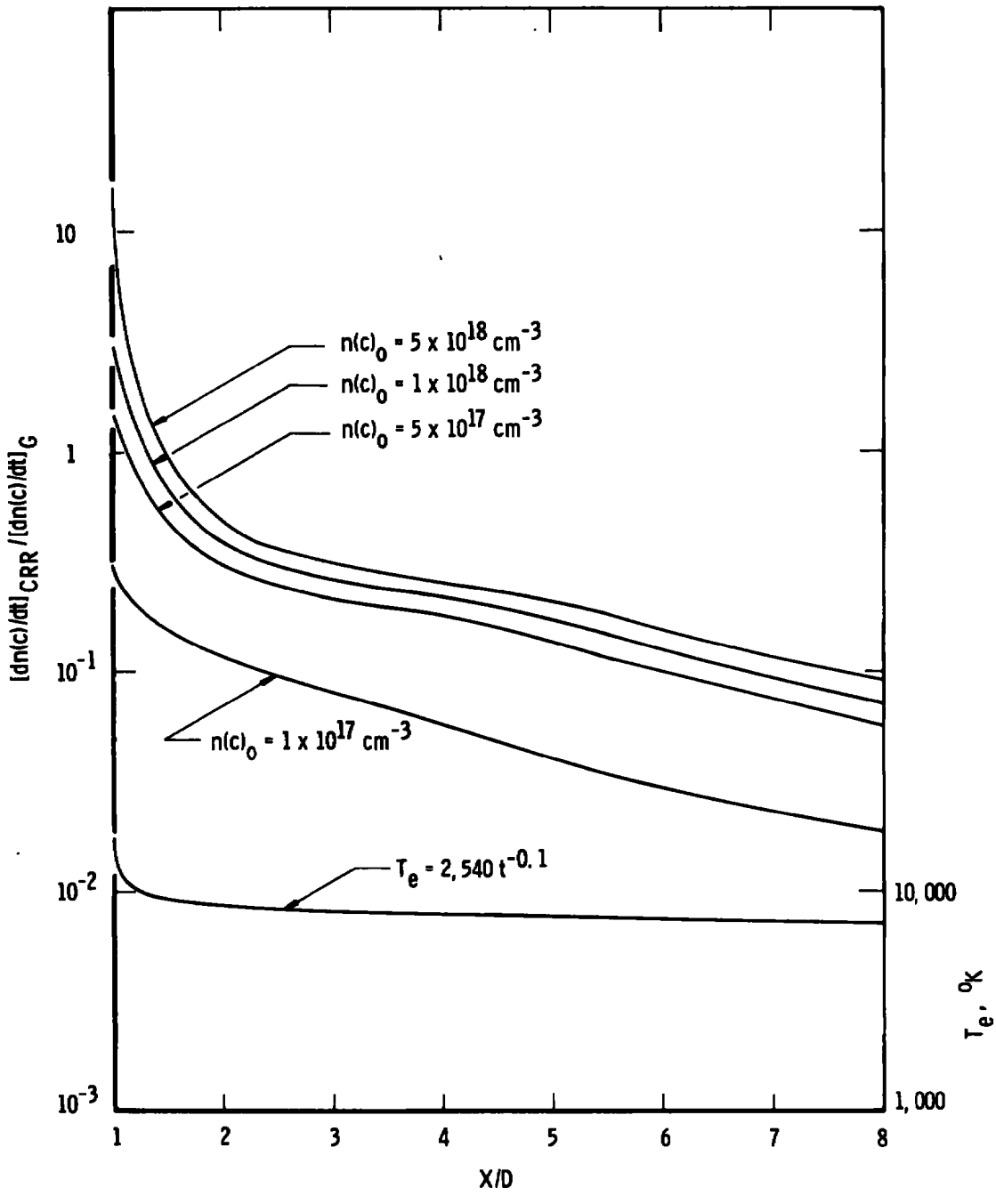

Figure 10. Comparison of electron number density decay rates attributable to recombination and gas dynamics, argon expansion, T_e modeled by slowly decaying function.

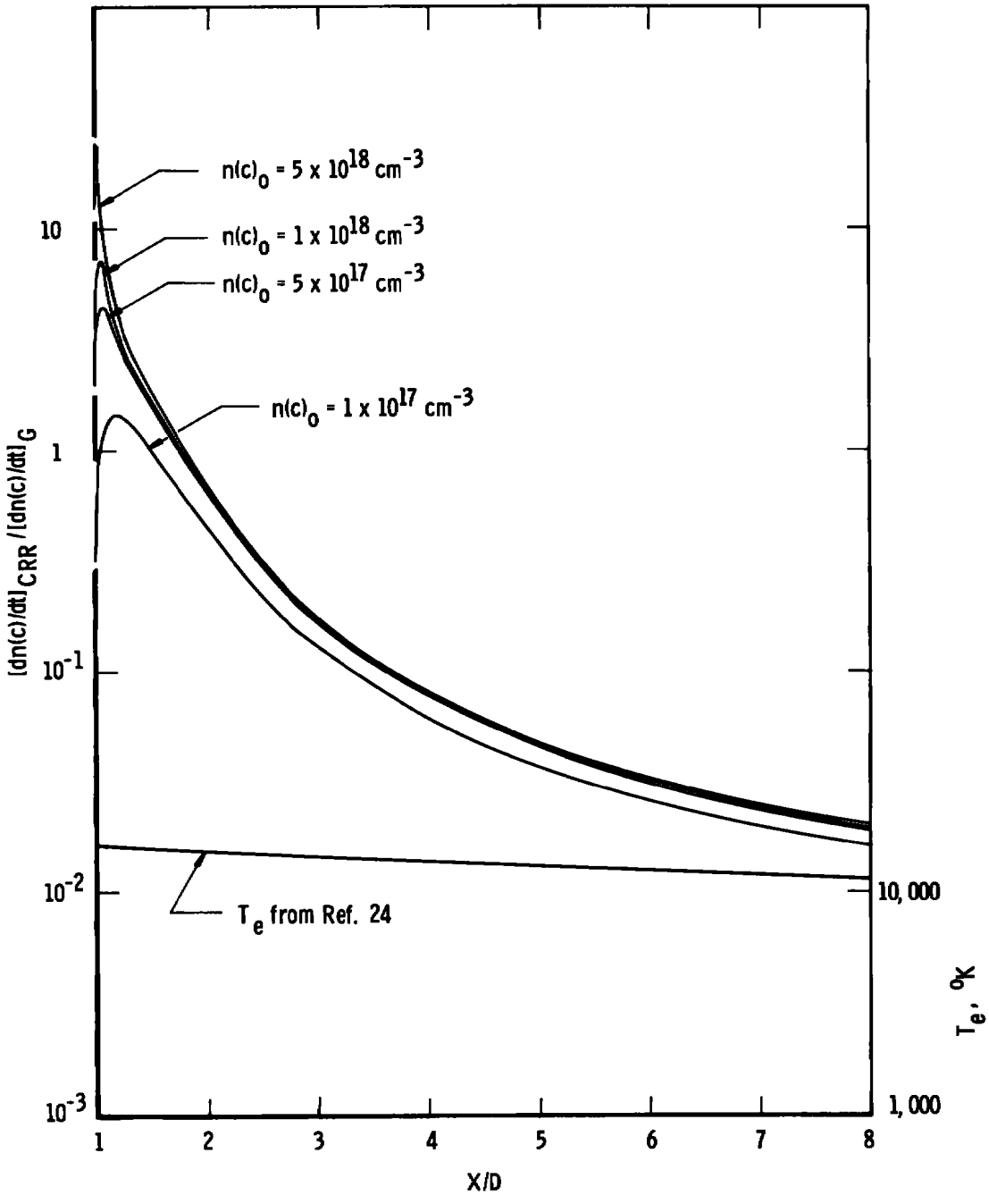

Figure 11. Comparison of electron number density decay rates attributable to recombination and gas dynamics, argon expansion, T_e modeled from Ref. 24.

into the test cell. The pressure in the test cell is maintained by two large mechanical vacuum pumps. A quartz window is mounted in the test cell for spectroscopic observations. In this study the arcjet nozzle had a diameter of 0.635 cm. A schematic representation of the test apparatus (not to scale), is shown in Fig. 12.

The chamber and lines were evacuated before arcjet operation in order to ensure minimum contamination. The argon gas supply was of 99.9-percent purity (with oxygen 1 ppm, nitrogen 1 ppm, hydrogen 1 ppm, and moisture 1 ppm) was supplied to the gas lines through a regulator adjusted to maintain a line pressure of 5,750 torr. The power supply to the arcjet was a motor generator providing an open line voltage of 85 v. The argon gas was introduced into the arcjet chamber and the plasma jet was started with an RF discharge of short duration which is used to break down the gas and then is shut off after the arc is started. Stable operating conditions were as follows:

Chamber pressure	142.2 torr
Gas flow	3.0 gm/sec
Operating amperage	200 amp
Operating voltage	25 v
Cell pressure	0.4 torr

A 1-m Jerrell-Ash spectrometer was placed so that the entrance slit (slit width of 18 μ) was aligned with the centerline of the nozzle in order to measure the intensities of spectral lines throughout the radial extent of the plasma, the spectrometer field of view was scanned across the plasma. This was accomplished by an optical system consisting of a converging lens with a focal length of 12 in. and a plane mirror. The mirror was rotated at an angular velocity of 72 deg/min to provide the scan of the field of view. The lens focused the light from the plasma onto the slit of the spectrometer. The detector was an RCA 1P28 photomultiplier tube which was connected to a Philbrick (model P2) amplifier. The gain on the amplifier was set at 100. The data were recorded on an x-y recorder.

After each scan the arcjet was lowered 0.635 cm and another scan was made. This procedure was continued until measurements of the intensity (radiated power per unit area per unit solid angle) of the selected spectral lines had been made at 0.635-cm intervals along the plume axis over a range of travel $3 \leq X/D < 6$. The 4158-Å spectral line and the 6032-Å spectral line were selected for the radial scans because reliable transition probabilities are available (Ref. 27) for these lines.

A calibrated tungsten filament lamp was used for calibration of the spectrometer and optical system as shown in Fig. 12. Table 3 lists the calibration scale factors for the two wavelengths (4158 Å and 6032 Å) that were used in this study. With these calibration values (which take into account the difference in using the tungsten source as compared to the plasma source) the numbers read from the traces on the x-y recorder can be given physically meaningful units. Thus the raw data are related to a true intensity of w/ster-cm^2.

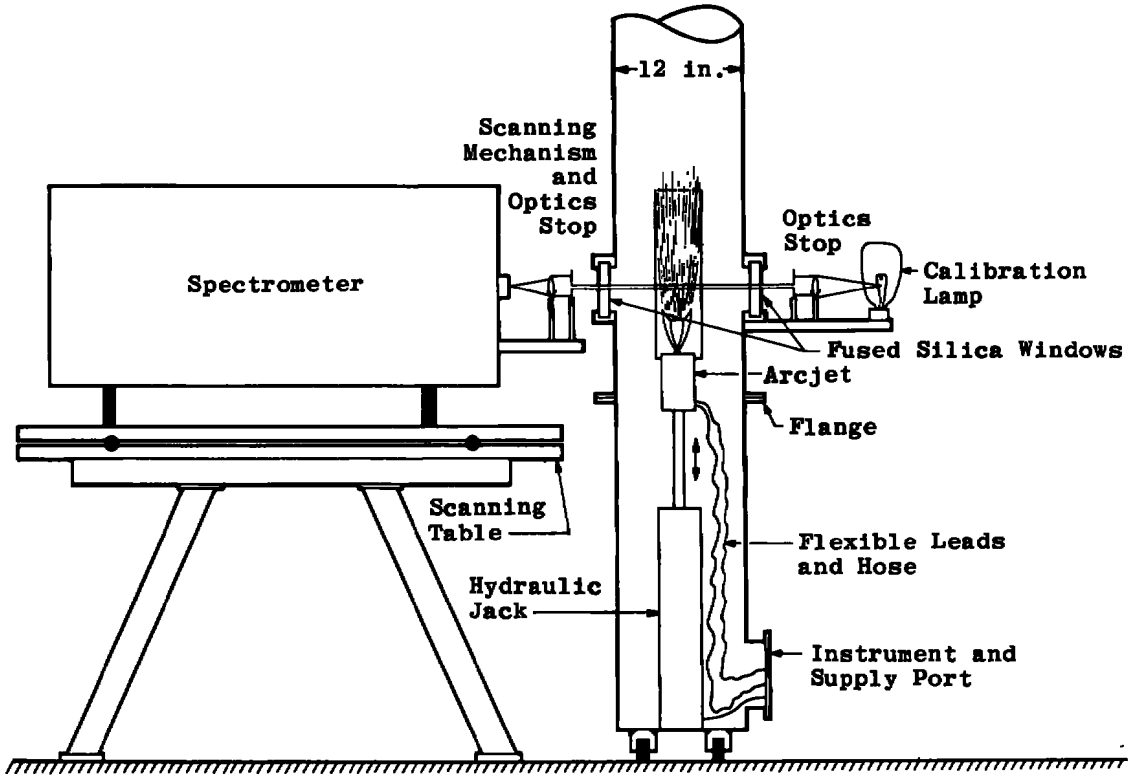

Figure 12. Research cell, plasma jet, and optics installation.

Table 3. Intensity Calibration Factors

X/D	Intensity, w/ster-cm^2/div	
	4158 Å	6032 Å
3.0	7.12×10^{-6}	3.63×10^{-6}
4.0	7.12×10^{-6}	3.73×10^{-6}
5.0	2.85×10^{-6}	1.87×10^{-6}

3.2.2 Data Analysis

Figures 13 through 18 are traces from the x-y recorder of the radiation intensities for both the 4158-Å line and the 6032-Å line that were used in this study for X/D = 3, 4, and 5. The plume was scanned at least twice for each spectral line at each axial position to verify arcjet stability and symmetry. The center of each peak corresponds to the location of the centerline of the plume, and the scans were examined for repeatiability and symmetry. In each case symmetry was satisfactory and the peak height was repeatable within 5 percent. The variations in the two scans were thus judged to be insignificant, and radiation intensity data as a function of distance from the centerline were obtained from one side of one scan only. These data were then converted to intensity units by the appropriate calibration factor given in Table 3.

The spectral line intensity measurements were used to obtain the local emission coefficients (radiated power per unit solid angle) by use of a computer code designed to effect the Abel inversion integral. The approach utilized in the code was, via a least-squares spline fit, to model the original intensity profiles with a series of polynomials of even powers of distance. The even function is chosen to ensure cylindrical symmetry, a requirement of the Abel inversion for this application. With the intensity modeled by the appropriate series of polynomials, the inversion is analytic and immediate. Figure 19 presents representative results of these inversions with the emission coefficient normalized by the centerline value for data at one of the points of measurement in this study.

Once the emission coefficients are calculated the electron temperature is determined with the assumption of local thermodynamic equilibrium (Ref. 28). The emission coefficient is divided by the statistical weight of the emitting state, the transition probability for the transition, and the frequency of the emitted radiation. The logarithm of this value is then plotted against the energy of the radiating state. These plots give nearly straight lines of slope $-0.4343/kT_e$, yielding immediately the electron temperature. In Fig. 20 is a plot of the electron temperature as determined from the emission coefficients along the centerline. The bars indicate the observed variation in the calculated electron temperature from variations in the fitted intensity data within the previously mentioned 5-percent variation.

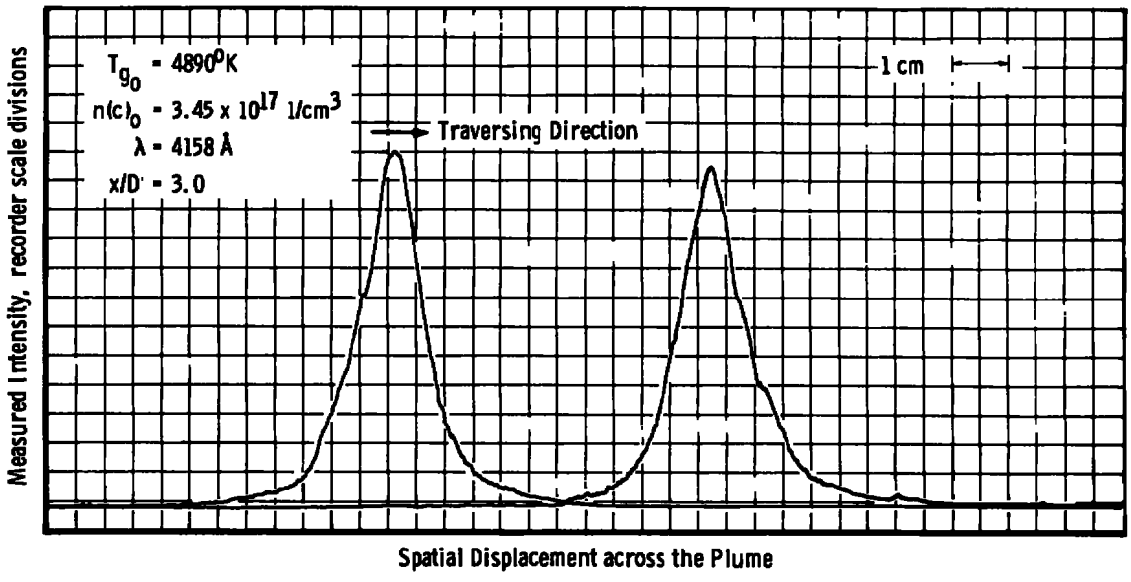

Figure 13. Radial plasma jet radiation intensity scans, X/D = 3, λ = 4158 Å.

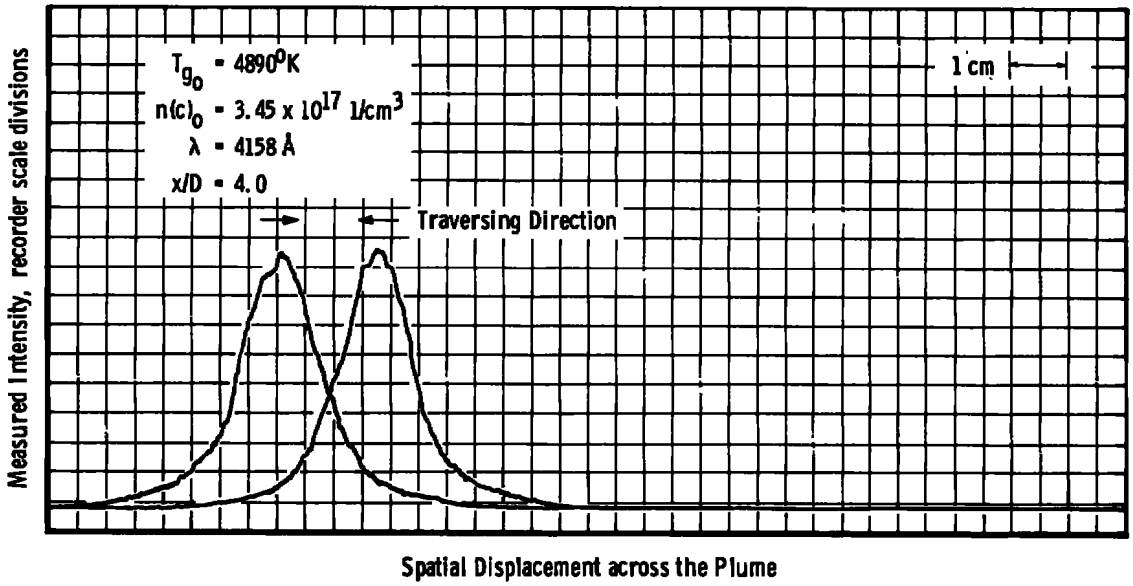

Figure 14. Radial plasma jet radiation intensity scans, X/D = 4, λ = 4158 Å.

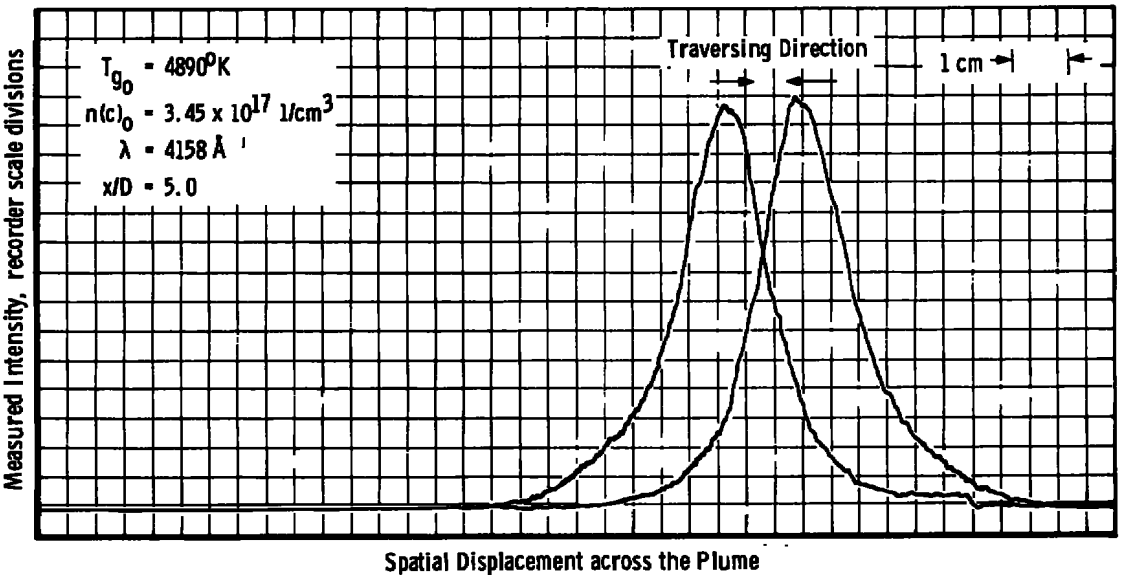

Figure 15. Radial plasma jet radiation intensity scans, X/D = 5, λ = 4158 Å.

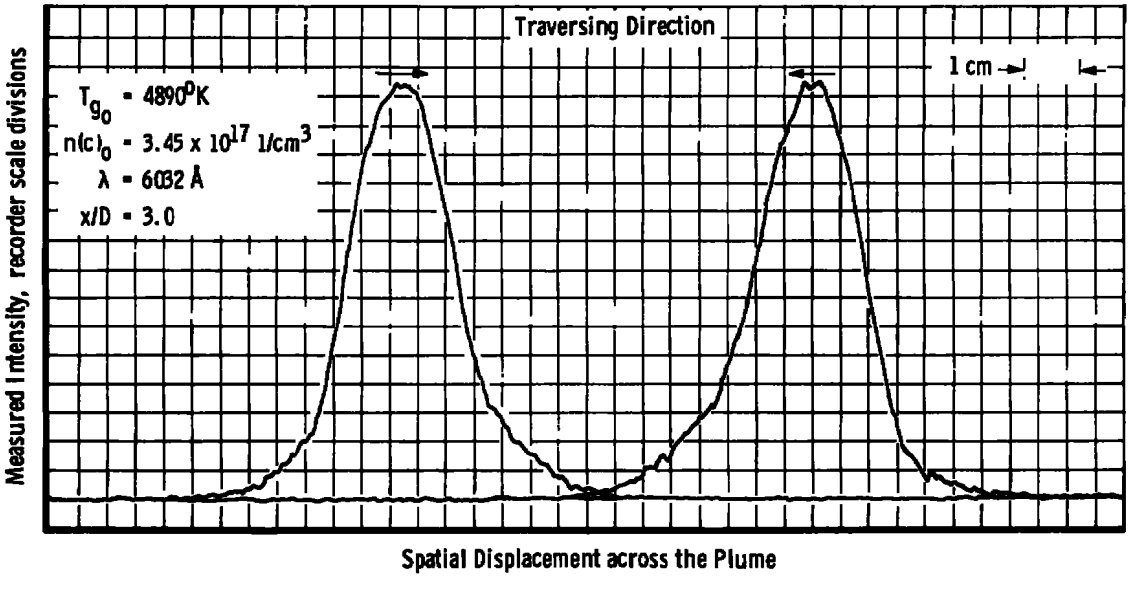

Figure 16. Radial plasma jet radiation intensity scans, X/D = 3, λ = 6032 Å.

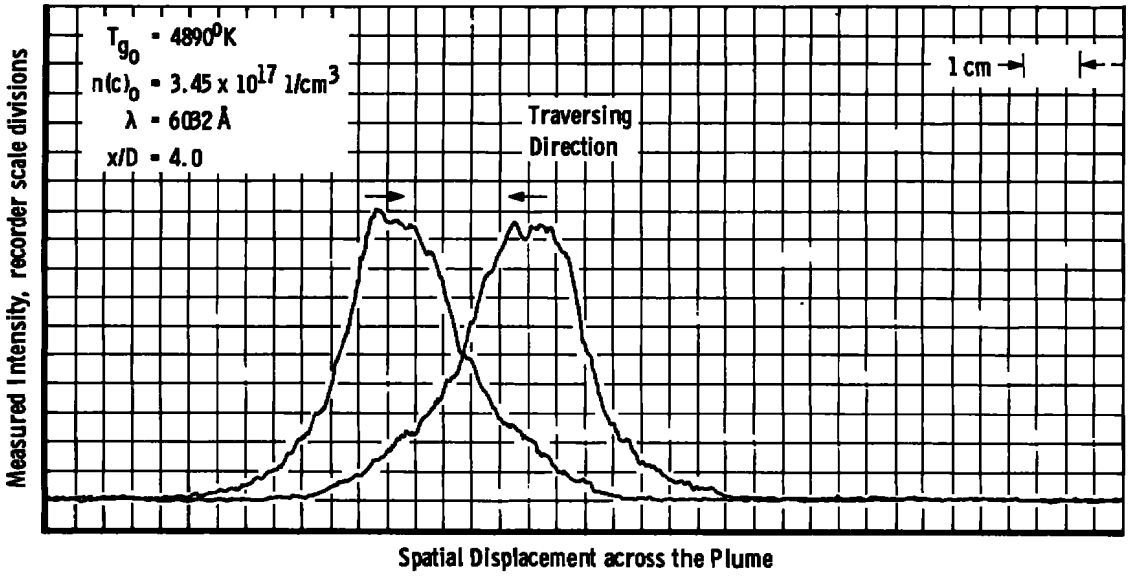

Figure 17. Radial plasma jet radiation intensity scans, X/D = 4, λ = 6032 Å.

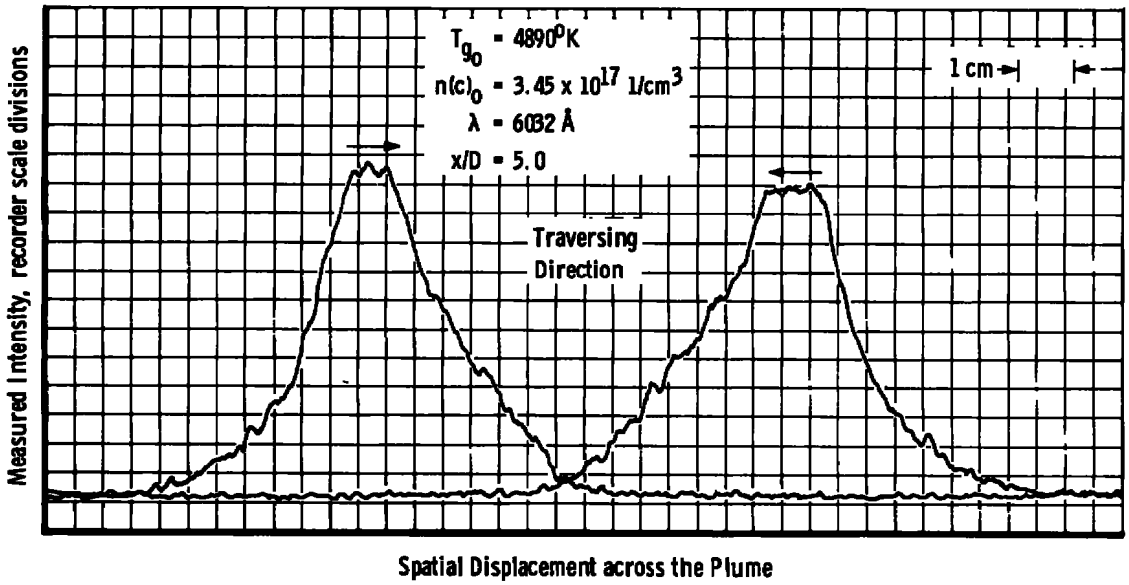

Figure 18. Radial plasma jet radiation intensity scans, X/D = 5, λ = 6032 Å.

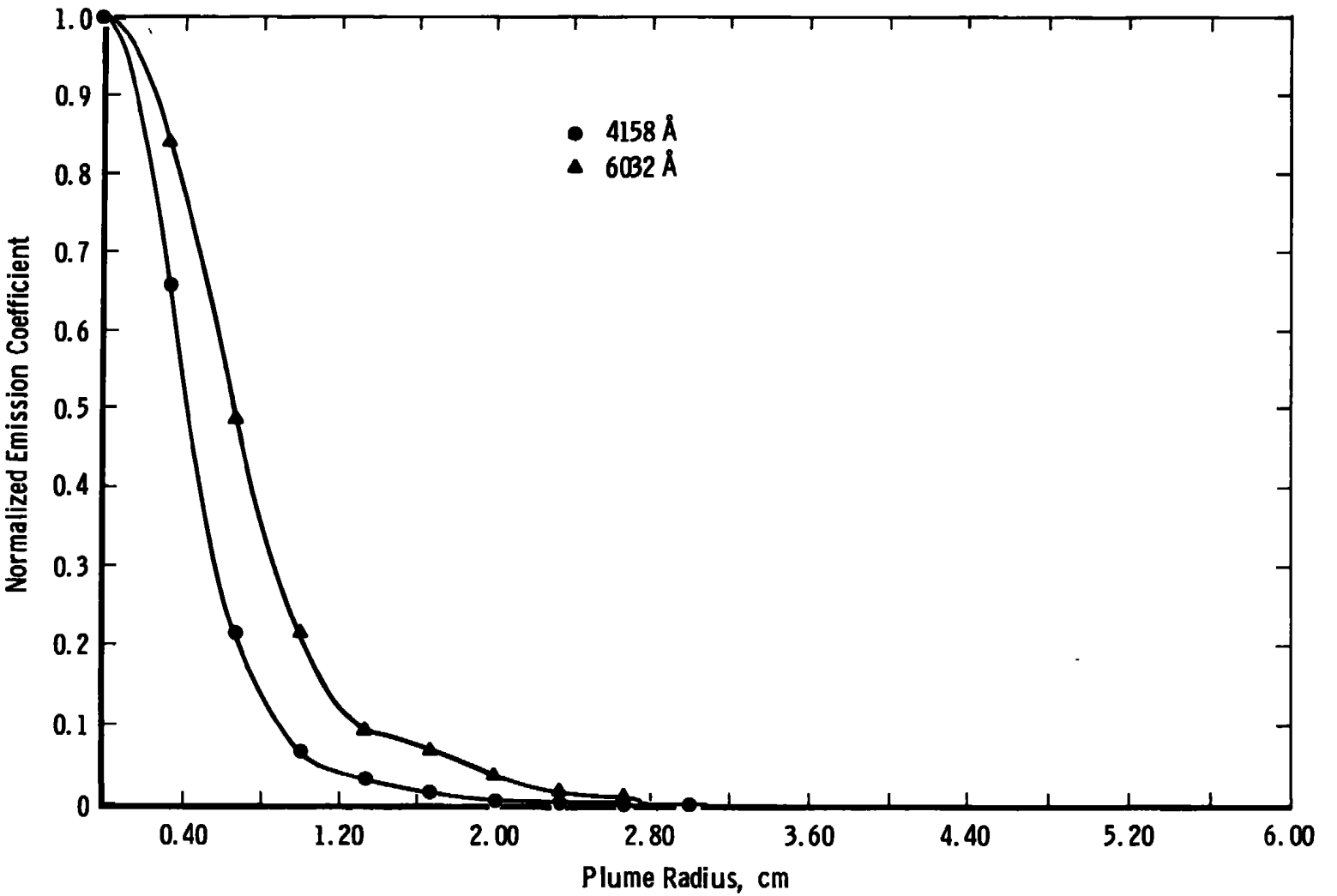

Figure 19. Normalized emission coefficient profiles, X/D = 3.

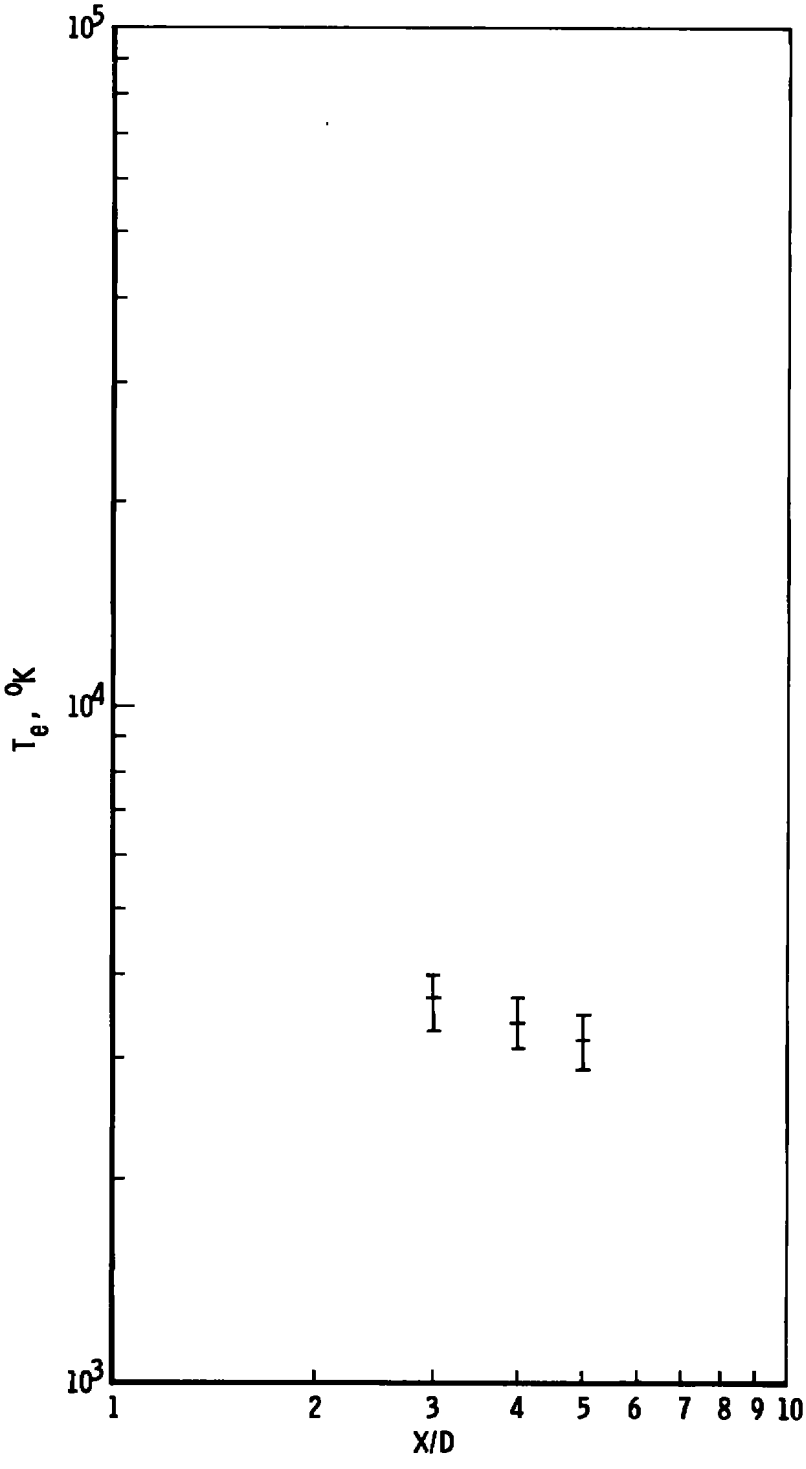

Figure 20. Plume centerline electron temperature as a function of X/D intensities $3 \leq X/D < 6$.

Since the gas is assumed to be singly ionized, the ion number density and electron number density are equal. Using the above determined T_e the n(c) can be determined from the principle of mass action (Saha's equation) by determining the n(c) in equilibrium with an excited state at the measured electron temperature (Ref. 28). These results are plotted in Fig. 21 for the electron number density along the centerline versus X/D. The bars in Fig. 21 have the same meaning as in Fig. 20. The three data points indicated in Fig. 21 can be connected with a straight line on the log-log plot. If gas-dynamic effects are the dominant feature of the electron density decay, potential flow theory demands that the n(c) decays according to an inverse square law, i.e., on a log-log plot such as Fig. 21, a straight line of slope -2 will result. If there are other completing phenomena for the electron density decay, such as the recombination process, these will be in addition to the gas-dynamic effects, and the log-log plot will necessarily have a slope steeper than -2. The straight line slopes obtained from Fig. 21 have a median value of -1.8 with lower and upper bounds of -1.45 and -2.15, respectively. Thus, one is led to the conclusion that the gas-dynamic effect is the principal contributor to the electron number density decay.

An alternate way to examine the relative effect of recombination and gas-dynamic expansion on the local electron number density is as follows. If the physical effects of the recombination process are to be observed in the experimental data, there should be a noticeable change in the ratio of the electron number density to atom number density as the distance from the nozzle exit increases. The ratio L given by

$$L = n(c)/n$$

is given in Table 4 for each of the three X/D positions, 3, 4, and 5. For these determinations the total number density was obtained from potential flow theory using stagnation conditions determined by applying Rayleigh heating relationships to the arcjet constant area anode (Ref. 23). Table 4 shows that, for each of the three positions, L is relatively constant with a variation of only approximately 8 percent. The almost constant value of L implies that the degree to which recombination is affecting the electron density must be very small compared to the gas expansion.

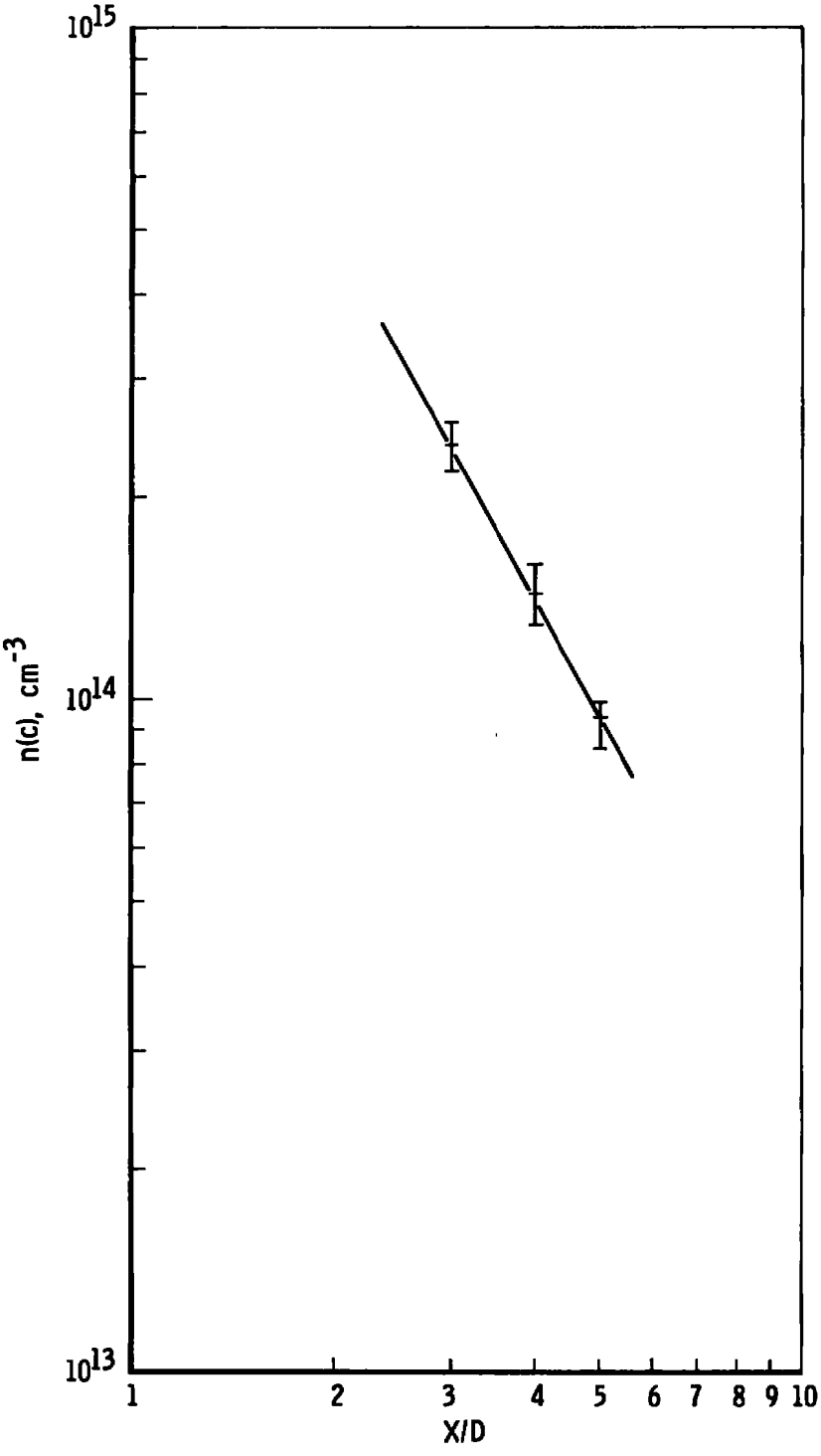

Figure 21. Plume centerline electron density profile as a function of X/D intensities $3 \leq X/D < 6$.

Table 4. Degree of Ionization at Appropriate X/D

X/D	n, cm^{-3}	n(c), cm^{-3}	L
3	2.42×10^{16}	2.39×10^{14}	9.88×10^{-3}
4	1.59×10^{16}	1.45×10^{14}	9.12×10^{-3}
5	1.02×10^{16}	9.47×10^{13}	9.29×10^{-3}

3.2.3 Comparisons with Theory

The results presented above have been consistent with the theoretical predictions and analysis presented in Section 3.1. However, the experimental data presented here were at a higher initial total gas temperature (4,890°K), whereas the electron number density (3.45×10^{17} cm^{-3}) was within the range of the conditions listed in Section 3.1. The higher gas temperature will affect principally the Mach number of the expansion and should not affect the general conclusion of Section 3.1 that gas-dynamic effects dominate the centerline rate of decay of n(c) for $X/D > 2$. However for completeness, the coupled recombination and gas-dynamic program was used with the above initial conditions in order to determine if the results of theory and experiment were indeed consistent. In Fig. 22 is a plot of the time rate of change of the free-electron number density attributable to gas-dynamic effects and recombination effects for the initial conditions of the experimental data versus time, and using the computation method described in Section 3.1.

The collisional-radiative recombination rate does dominate in the region $X/D < 2$. However, in the practical sense this portion is inaccessible because of the blown arc which protrudes to about $X/D = 2$ and causes the assumptions of a field free expansion to be invalidated. In the region ($3.0 \leq X/D < 6.0$) where analysis of the data is justifiable the gas-dynamic rate dominates, which is consistent with the theoretical work of Section 2.1 and the analysis of the experimental data presented in this Section.

4.0 SUMMARY AND CONCLUDING REMARKS

This work has provided a study of the electron number densities and recombination rates to be expected along the centerline of the freely expanding plume from an argon or helium arcjet. The purpose of the

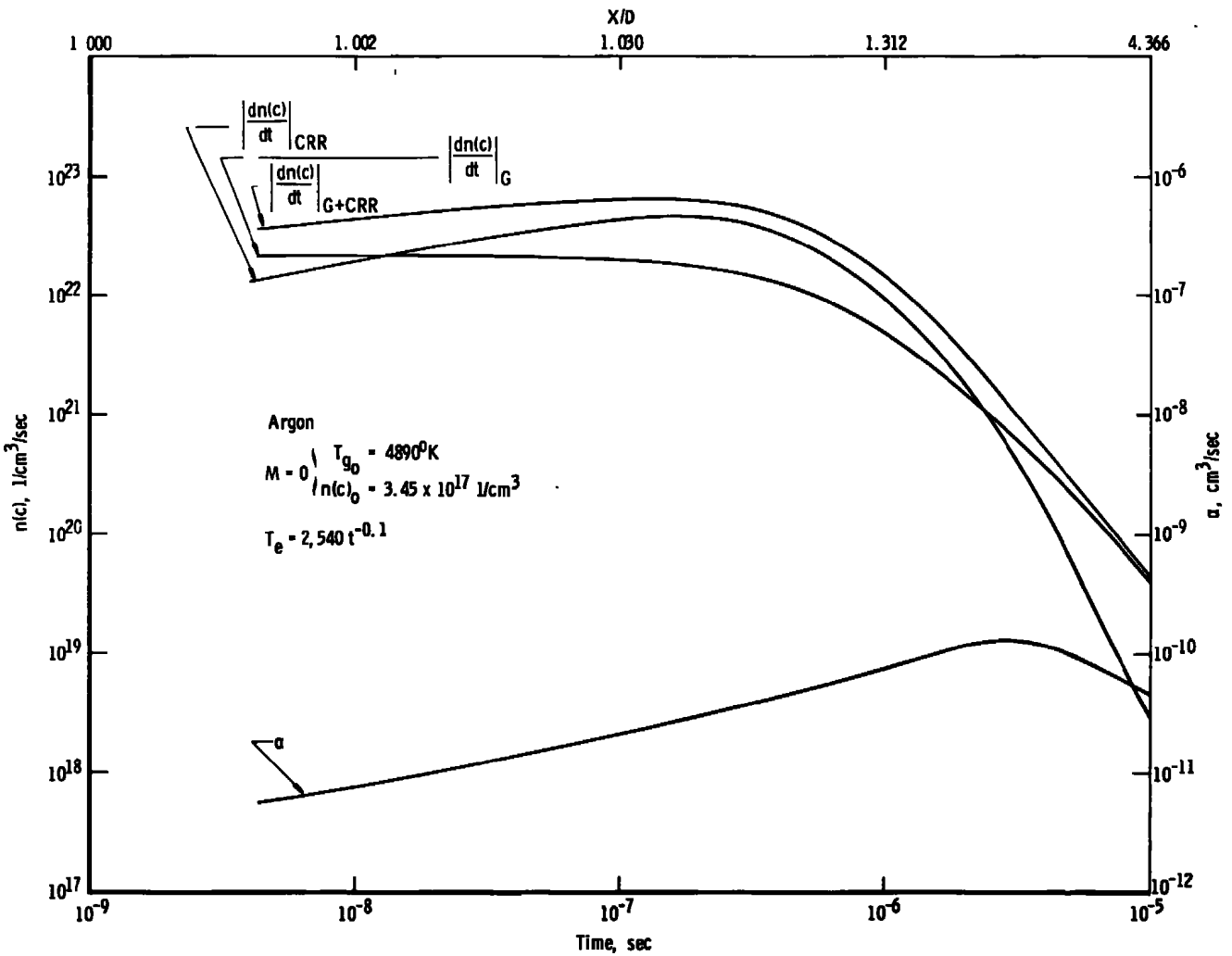

Figure 22. Time development of electron density decay rates for the argon expansion experiment.

study was to examine the relative rates of decay of the free-electron number density attributable to the recombination processes and the gas-dynamic processes. For this purpose the equations describing the recombination process were superposed with the equations describing the free isentropic expansion of an ideal gas. In this manner, calculations comparing the rate of change of the free-electron number density caused by recombination to the rate of change caused by the gas-dynamic expansion were made for a range of conditions similar to those anticipated for a typical arcjet plume.

In the range of stagnation conditions studied ($3,000°K \leq$ total gas temperature $\leq 4,900°K$; 1×10^{17} cm$^{-3} \leq$ electron number density $\leq 5.00 \times 10^{18}$ cm^{-3}; and $1,200°K \leq$ electron temperature $\leq 20,000°K$) the gas-dynamic rate of decay of the free-electron number density generally dominated the recombination rate. It was further found that those conditions for which the recombination rate did dominate over the gas-dynamic rate of decay of the free-electron number density required electron densities which are in the range of, but are generally greater than, those normally achieved in typical arcjet experiments. Further, this domination by recombination processes occurs only for a short distance downstream of the nozzle exit, $X/D < 2$. Analysis of available experimental data confirmed these calculated results. This data analysis showed that the electron number density decay along the centerline of the plume was functionally an inverse square dependence, as is required by potential flow theory, and further, that the degree of ionization was very nearly constant as a function of axial distance from the arcjet nozzle. This latter result is further evidence that the recombination process did not affect the electron density appreciably in the region studied, as it would have if it were an important feature of the decay.

It is thus concluded that determinations of the electron number density in the expanding plume of the arcjet will reflect the effect of the gas-dynamic expansion rather than the contribution of the recombination mechanisms. Hence, the arcjet plume cannot be used for direct determination of the recombination rate coefficient from the electron number density. Rather, a previous approach, described in Ref. 11, which requires detailed spectral intensity and/or absorption measurements to determine the excited state distribution function should be used. These detailed intensity measurements will not only provide means to determine the recombination rate coefficients, but also the means to examine the fully transient plasma decay problem (Ref. 16). These studies could be accomplished without recourse to the simplfying quasi-steady-state assumption used here.

REFERENCES

1. McDaniel, E. W. Collision Phenomena in Ionized Gases. John Wiley and Sons, Inc., New York, 1964.
2. Biondi, M. A. and Brown, S. C. "Measurements of Ambipolar Diffusion in Helium." Physical Review, Vol. 75, June 1949, pp. 1700-1705.
3. Biondi, M. A. and Brown, S. C. "Measurements of Electron-Ion Recombination." Physical Review, Vol. 76, December 1949, pp. 1697-1700.
4. Oskam, H. J. "Microwave Investigation of Disintegrating Gaseous Discharge Plasmas." Philips Research Report, Vol. 13, August 1958, pp. 335-400.
5. Redfield, A. and Holt, R. B. "Electron Removal in Argon Afterglows." Physical Review, Vol. 82, June 1951, pp. 874-876.
6. Oskam, H. J. and Mittelstadt, V. R. "Recombination Coefficient of Molecular Rare-Gas Ions." Physical Review, Vol. 132, November 1963, pp. 1445-1454.
7. Chen, C. J. "Collisional-Radiative Electron-Ion Recombination Rate in Rare-Gas Plasmas." Journal of Chemical Physics, Vol. 50, February 1969, pp. 1560-1566.
8. Chen, C. J. "Partition of Recombination Energy in the Decaying Rare-Gas Plasmas." Physical Review, Vol. 163, November 1967, pp. 1-7.
9. Gusinow, M. A., Gerardo, J. B., and Verdeyen, J. T. "Investigation of Electron Recombination in Helium and Argon Afterglow Plasmas by Means of Laser Interferometric Measurements." Physical Review, Vol. 149, September 1966, pp. 91-96.
10. Gerardo, J. B. and Verdeyen, J. T. "Correlated Interferometric Measurements of Plasma Electron Densities at Optical and Microwave Frequencies." Applied Physics Letters, Vol. 6, May 1965, pp. 105-107.
11. Shirai, H. and Tabei, K. "Measurements of the Electronic Recombination Coefficient in a Helium Plasma Jet." Physical Review A, Vol. 7, April 1973, pp. 1402-1407.

12. Byron, S., Stabler, R. C., and Bortz, P. I. "Electron-Ion Recombination by Collisional and Radiative Processes." Physical Review Letters, Vol. 8, May 1962, pp. 376-379.

13. Bates, D. R., Kingston, A. E., and McWhirter, R. W. P. "Recombination Between Electrons and Atomic Ions." Proceedings of the Physical Society of London, Vol. 267 (Series), May 1962, pp. 297-312.

14. Drawin, H. W. and Emaid, F. "Collisional-Radiative Volume Recombination and Ionization Coefficients for Quasi-Stationary Helium Plasmas." Z. Phys. k, Vol. 243, 1971, pp. 326-340.

15. Wanless, D. "Electron-Ion Recombination in Argon." Journal of Physics B: Atomic and Molecular Physics, Vol. 4, April 1971, pp. 522-527.

16. Limbaugh, C. C. "The Transient Behavior of Collisional-Radiative Recombination in Atomic Helium Plasmas." Ph. D. Dissertation, University of Tennessee, Knoxville, Tennessee, 1971.

17. Bryson, R. J. and Fröhlich, J. P. "Study of the Energy Addition Process in a D-C Arc Jet." AEDC-TR-65-268 (AD631591), Arnold Air Force Station, Tennessee, April 1966.

18. Shapiro, A. H. The Dynamics and Thermodynamics of Compressible Fluid Flow. Vol. I. The Ronald Press Company, New York, 1954.

19. White, A. B. "Part I. Experimental Investigation of Arc-Heated Supersonic Free Jet. Part II. Analysis of One-Dimensional Isentropic Flow for Partially Ionized Argon." Ph. D. Dissertation, California Institute of Technology, Pasadena, 1967.

20. Ashkenas, H. and Sherman, F. S. "The Structure and Utilization of Supersonic Free Jets in Low Density Wind Tunnels." Rarefied Gas Dynamics, J. H. de Leeuw, editor. Supplement 3, Vol. II. Academic Press, Inc., New York, 1966, pp. 84-105.

21. Fröhlich, J. P., Staats, G. E., and McGregor, W. K. "Gas Dynamic Analysis of an Arc-Heated Plasma Facility." AEDC-TR-67-168 (AD820798), Arnold Air Force Station, Tennessee, October 1971.

22. Bryson, R. J. "Anode Nozzle Effects on the Bulk Properties of Arc-Heated Argon." AEDC-TR-68-106 (AD670511), Arnold Air Force Station, Tennessee, June 1968.

23. Bryson, R. J. "A Method for Determining the Bulk Properties of Arc-Heated Argon." AEDC-TR-69-125 (AD689178), Arnold Air Force Station, Tennessee, June 1969.

24. McGregor, W. K. and Brewer, L. E. "Equivalence of Electron and Excitation Temperatures in an Argon Plasma." Research Notes, The Physics of Fluids, Vol. 9, April 1966, pp. 826-826.

25. Brewer, L. E. "Plasma Radiation Resulting from an Over-population of Atoms in the Metastable State." Master's Thesis, The University of Tennessee, Knoxville, 1965.

26. McGregor, W. K. "Examination of the Conservation Laws in a Particular Class of Collisions of the Second Kind." Ph. D. Dissertation, The University of Tennessee, Knoxville, 1969.

27. Wiese, W. L., Smith, M. W., and Glennon, B. M. Atomic Transition Probabilities, Vol. II., National Bureau of Standards, United States Department of Commerce. Government Printing Office, Washington, 1969.

28. Griem, H. R. Plasma Spectroscopy. McGraw Hill Book Co., New York, 1964.

NOMENCLATURE

A	Empirical constant
A(p, q)	Transition probability from p to q sec^{-1}
C	Empirical constant
c	Speed of sound, cm/sec
D	Diameter of nozzle, cm
e	Charge on electron, 4.80286×10^{-10} stat coulomb
e^-	Electron
h	Planck's constant, 6.62517×10^{-27} ergs-sec
K(c, p)	Rate coefficient for three-body recombination into quantum state p, cm^3/sec
K(p, c)	Rate coefficient for collisional ionization by electrons from quantum state p, cm^3/sec
K(p, q)	Rate coefficient for excitation or de-excitation from level p to level q, cm^3/sec
k	Boltzmann's constant, 8.6164×10^{-5} eV/°K
L	Level of ionization
M	Mach number
N^+	Singly ionized atom
n	Neutral atom number density, cm^{-3}
n(c)	Electron number density, cm^{-3}
$n(N^+)$	Ion number density, cm^{-3}
n(p)	Number density of atoms in quantum state p, cm^{-3}
p, q	Symbolic for set of quantum numbers defining energy levels
R	Gas constant, erg/(g-mole)/°K
S	Collisional-radiative ionization coefficient, cm^3/sec
T_e	Electron temperature, °K

T_g	Gas temperature, °K
t	Time, sec
$\overline{\Delta t}$	Average elapsed time, sec
V	Velocity of flow, cm/sec
X	Distance from nozzle along centerline, cm
X_o/D	Nondimensional geometric constant
Z	Refers to the level of ionization
α	Collisional-radiative recombination rate coefficient, cm^3/sec
$\beta(p)$	Rate coefficient for radiative recombination into quantum state p, cm^3/sec
Γ	Collisional-radiative decay coefficient, cm^3/sec
γ	Ratio of specific heats
λ	Wavelength, cm
ν	Frequency, 1/sec
ρ	Mass density, g/cm^3

SUBSCRIPTS

1, 2	Refers to two points in the flow along the centerline
CRR	Refers to collisional-radiative recombination contributions only
G	Refers to gas-dynamic contributions only
o	Refers to stagnation values or starting position